ACS OMEGA

Open Access

http://pubs.acs.org/journal/acsodf

Article

Application of a Novel Green Nano Polymer for Chemical EOR Purposes in Sandstone Reservoirs: Synergetic Effects of Different Fluid/Fluid and Rock/Fluid Interacting Mechanisms

Abbas Khaksar Manshad, Alireza Kabipour, Erfan Mohammadian,* Lei Yan, Jagar A. Ali, Stefan Iglauer, Alireza Keshavarz, Milad Norouzpour, Amin Azdarpour, S. Mohammad Sajadi, and Siyamak Moradi

Cite This: *ACS Omega* 2023, 8, 43930−43954

Read Online

ACCESS | Metrics & More | Article Recommendations

ABSTRACT: In this research, a novel natural-based polymer, the Aloe Vera biopolymer, is used to improve the mobility of the injected water. Unlike most synthetic chemical polymers used for chemical-enhanced oil recovery, the Aloe Vera biopolymer is environmentally friendly, thermally stable in reservoir conditions, and compatible with reservoir rock and fluids. In addition, the efficiency of the Aloe Vera biopolymer was investigated in the presence of a new synthetic nanocomposite composed of KCl−SiO_2−xanthan. This chemically enhanced oil recovery method was applied on a sandstone reservoir in Southwest Iran with crude oil with an API gravity of 22°. The Aloe Vera biopolymer's physicochemical characteristics were initially examined using different analytical instruments. The results showed that the Aloe Vera biopolymer is thermally stable under reservoir conditions. In addition, no precipitation occurred with the formation brine at the salinity of 80,000 ppm. The experimental results showed that adding ethanol with a 10% volume percentage reduced interfacial tension to 15.3 mN/m and contact angle to 108°, which was 52.33 and 55.56% of these values, respectively. On the other hand, adding nanocomposite lowered interfacial tension and contact angle values to 4 mN/m and 48°, corresponding to reducing these values by 87.53 and 71.42%, respectively. The rheology results showed that the solutions prepared by Aloe Vera biopolymer, ethanol, and nanocomposite were Newtonian and fitted to the Herschel−Bulkley model. Finally, core flooding results showed that the application of a solution prepared by Aloe Vera biopolymer, ethanol, and nanocomposite was effective in increasing the oil recovery factor, where the maximum oil recovery factor of 73.35% was achieved, which could be attributed to the IFT reduction, wettability alteration, and mobility improvement mechanisms.

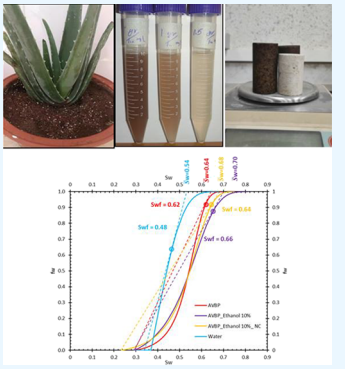

1. INTRODUCTION

Natural oil and gas are still among humans' most essential energy sources. Enhanced oil recovery (EOR) methods have been frequently used to maintain and increase the efficiency of these hydrocarbon resources. Various geological structures in these reservoirs usually cause variations in the petrophysical parameters. These variations are scattered in reservoirs, and sometimes, significant changes in porosity or permeability may be observed at short distances. These variations and the uneven distribution of the parameters lead to suboptimal performance of EOR processes, such as water injection.[1−7] Most EOR processes are water-based; hence, some factors, such as heterogeneity in porosity and permeability, adversely affect the sweep efficiency of water-based EOR processes and eventually result in high water cut and fingering problems. It is widely accepted that the proper injection scenario through the use of suitable chemicals can markedly increase the efficiency of the process. If the desired displacing fluids (polymers, surfactants, nanomaterials, etc.) fail to reach all reservoir parts uniformly, then the EOR process will have a low sweep efficiency. Thanks to their higher viscosity compared to water, polymers are widely used to alleviate the low mobility issues of the injection front.[8−11] Extensive studies have been performed in the polymers' fields, and it has always been tried to synthesize stable polymeric materials under reservoir temperature and pressure conditions. The stability of the polymers under high salinity conditions is one of the critical challenges in chemically enhanced oil recovery (CEOR) processes. The second important consideration when using polymers is their absorption into reservoir rocks. This issue increases the total polymer consumption and, in turn, elevates the cost of the CEOR projects. In addition, from the point of view of environmental impacts, the growing concerns about the use of chemical materials and their potential effects on the environ-

Received: August 11, 2023
Revised: October 20, 2023
Accepted: October 24, 2023
Published: November 13, 2023

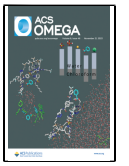

Table 1. Summary of the Efficiencies of the CEOR Methods Used in the Literature and This Study

material	additive	optimization			ref.
		IFT		recovery Factor	
SiO_2	ethanol	93%	29%	23.0%	19
	PAM	62%		24.7%	25
	xanthan gum	64%	76%	7.81%	26
	LSW	34%	40%	10.1%	27
	brine	60%	70%	28.0%	28
TiO_2	water		28%	21.0%	29
	polymer			31.0%	30,31
TiO_2/SiO_2	DIW	66%	65%	26.0%	32
anionic surfactant: poultry wastes	DIW; 75 °C	96%	72%	17.8%	33
	NaCl; 75 °C	97%			
	alkali; 75 °C	98%			
preformed particle gel (PPG)	DIW		64%	15.3%	34
midazolium-based ionic liquids	FW	75%			35
	SW	41%			35
SiO_2@Montmorillonite@Xanthan	DIW	56%	78%	11.8%	36
Aloe Vera biopolymer (AVBP)	**DIW**	**24%**	**23%**	**7.99%**	**this study**
	ethanol	**53%**	**55%**	**17.93%**	**this study**
	ethanol/nanocomposite (NC)	**88%**	**72%**	**24.13%**	**this study**

ment require industries to minimize the risk of leakage or release of nonbiodegradable polymers. Therefore, biobased polymers will soon get more attention for CEOR applications.[1,12−14]

Cellulose and starches are two great sources of natural polymers. Their availability, low cost, abundance, biodegradability, and nontoxicity make them suitable raw materials for polymer production. In addition, they are resistant to harsh reservoir conditions based on the long polysaccharide chains and resilient structure. Previous studies have demonstrated the adequate performance of natural polymers in CEOR applications. *Brachystegia eurycoma*, cassava starch, exudate gum, gum Arabic, and *schizophyllan* are some natural polymers tested in the lab as potential CEOR agents.[14−18]

Roustaei et al.[19] investigated the efficiency of the polysilicon nanoparticles for EOR. In order to prepare these nanoparticles, they used ethanol and the efficiency of these nanoparticles was explored through contact angle (CA), interfacial tension (IFT), and oil recovery measurement in sandstone reservoirs. They concluded that the primary mechanisms for improving oil recovery with these nanoparticles are IFT and CA reduction, where minimum IFT and CA values of 1.75 mN/m and 81.88° were achieved, respectively. In addition, a maximum oil recovery of 32.2% was achieved by injecting these nanoparticles into the core samples.

Goudarzi et al.[20] used an environmentally friendly polymer called "super absorbent" for zone plugging purposes and flow diversion. Their study focused on significantly fractured high-permeability reservoirs with an increased permeability difference between the matrix and fractures. They employed a combination of absorbent polymers and smart water flooding and achieved a recovery factor of 81%. They also reported that their polymer has sufficient stability under reservoir temperature and pressure conditions. In addition, they could divert injected fluid toward unswept areas with lower permeability and increase the recovery factor. One of the negative drawbacks of this study was that the application of this polymer was examined only in sandstone reservoirs and its efficiency for the carbonate reservoirs was not examined. Therefore, it is crucial to perform a thorough study and examine the efficiency of these compounds in carbonate reservoirs.

Furthermore, some research has also been conducted on plant-based polymers. One of the main advantages of these materials is that they are entirely natural. Moreover, simple chemical methods are usually optional for extraction.[21,22] Nowrouzi et al.[23] derived a natural polymer from the *Hollyhocks* plant and determined the optimum concentration in the presence of alkaline. The alkaline-polymer slug was injected into a sandstone core, increasing the recovery factor to 81.1% from an initial value of 53.2%. In addition, the natural polymer lost only 9% of its initial weight up to 129 °C, showing an improved thermal stability. One of the drawbacks of their study was that they used a low-asphaltene crude oil with an asphaltene content of 2.3%. In addition, they used sandstone core samples in their research. Therefore, the efficiency of this natural polymer could be further evaluated in the presence of high-asphaltene-content crude oil and carbonate core samples.

Ahmadi et al.[24] used green polymeric nanocomposites for EOR in a carbonate oil reservoir. In their study, xanthan/magnetite/SiO_2 nanocomposites (NC), eucalyptus plant nanocomposites (ENCs), and walnut shell ones (WNC) were used and their efficiency for EOR was examined through IFT and CA measurement as well as spontaneous imbibition tests. They concluded that one of the significant advantages of these materials is that they are very cost-effective and efficient, with low concentrations of 0.05 wt % at reservoir conditions. In addition, the primary mechanism for EOR with these green materials is due to IFT and CA reduction.

In another study performed by Ahmadi et al.,[12] the efficiency of the ZnO/SiO_2/xanthan as new NCs was compared with commercial SiO_2 nanoparticles. Their results showed that green polymer NCs were more effective than SiO_2 nanoparticles in lowering the IFT and CA. In addition, the polymer NC was very stable at high-salinity conditions, where additional oil recoveries of 25.1 and 34.1% were achieved with 25 times diluted seawater (25 SW) and 10 times diluted seawater (10 SW), respectively. Table 1 summarizes the results of some of the previous CEOR studies. Table 1 presents the

https://doi.org/10.1021/acsomega.3c05921
ACS Omega 2023, 8, 43930−43954

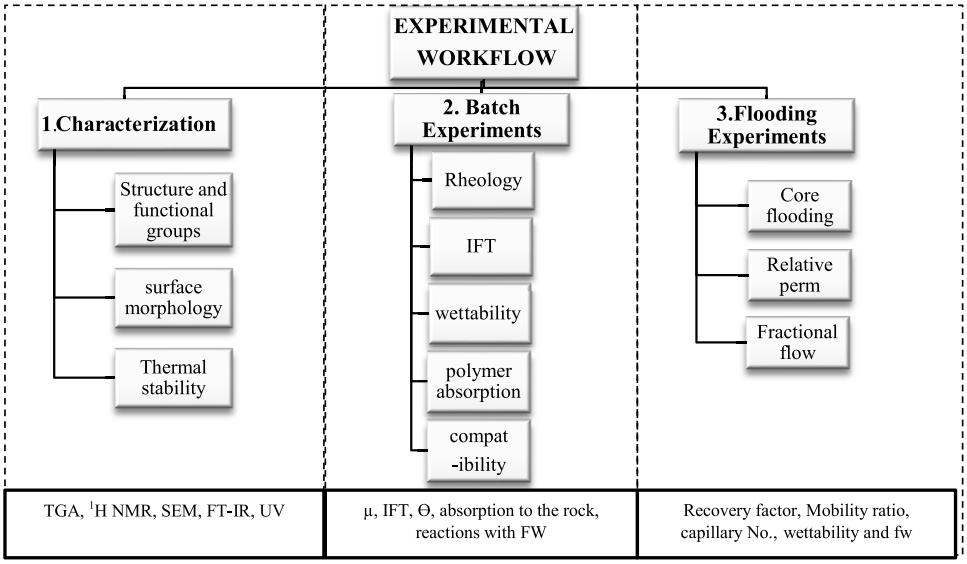

Figure 1. Experimental workflow of this study.

use of different chemicals and their effects on the IFT, CA (θ), and recovery factor (RF) parameters in some previous studies and those used in this research.

Several parameters should be considered when selecting a polymer for CEOR applications, including stability under high-temperature and high-salinity conditions, low rock surface absorption, and adequate rheological properties. Considering the properties of polymers can help to select a suitable injecting fluid that potentially results in optimum recoveries. However, there is little available research in which all those factors are addressed.[37−39] In addition to being environmentally friendly, the polymer should be compatible with the formation brine and reservoir rock, in which it will be injected. For this purpose, in this research we tried to conduct a comprehensive study on the performance of a natural polymer for CEOR purposes. Initially, the characteristics of the AVBP polymer were comprehensively investigated by using various standard analyses, including Fourier-transform infrared spectroscopy (FTIR), thermogravimetric analysis (TGA), nuclear magnetic resonance (NMR), and scanning electron microscopy (SEM) techniques. The next part measures the rheology properties of the solutions prepared by AVBP. Then, the IFT and CA values of polymer, polymer−ethanol, and polymer−ethanol−NC solutions were measured. Afterward, a solution prepared by an optimal concentration of polymer, ethanol, and NC is prepared and the RF with this solution is examined through core flooding experiments. Finally, the capillary number, mobility ratio, and relative permeability are measured under different scenarios. The overall workflow of the experimental procedure used in this study is shown in Figure 1.

2. MATERIALS AND METHODS

2.1. Materials. *2.1.1. Crude Oil, Brine, and Ethanol Sources.* Milli-Q-filtered (18.2 Ω) distilled water was used in this study to prepare all of the solutions. The formation water (FW) was collected from a reservoir in southwestern Iran. The FW has a total dissolved salinity (TDS) of 174,500 (mg/L) and is mainly saturated with Na^+, Cl^-, and SO_4^{-2} ions. Table 2 presents the composition of the FW used in this study. The crude oil used in this study is dead oil with an API gravity of 22° and a viscosity of 34.1 cp, which is obtained from a reservoir in southwestern Iran. The properties and percentages of the components of this crude oil are given in Table 3. The ethanol used in the study was purchased from a local manufacturer and used without further alteration, and it has a density of 789 kg/m^3 and a purity of 99.8%.

Table 2. FW Analysis Used in This Study

component	concentration (mg/L)
K^+	660
Na^+	66,000
Ca^{2+}	660
Mg^{2+}	1,400
SO_4^{-2}	20,000
Cl^-	85,000
HCO_3^{-2}	960
Total	**174,500**

2.1.2. Aloe Vera Plant. The AVBP powder with polymeric properties was extracted from the Aloe barbadensis miller plant cultivated in south Iran. To prepare the AVBP plant, it was washed, cut, and soaked in DIW for 24 h to enable mucilage extraction. The extracted solution was then filtered and concentrated using a vacuum dryer operating at 40 °C and 90 rpm. The resulting concentrated mucilage was the one to be used to prepare polymer solutions at 0.1, 1, and 2 g/100 mL in the current study. Figure 2 illustrates the plant and extracted powder. The extracted powder was in the form of fine grains of light-brown powder extracted using the mucilage extraction method. The extraction method is explained in detail in the work of Ling et al.[18] Table 4 shows some characteristics of the AVBP powder used in this study.

2.1.3. NC. A new synthetic NC used in this study is composed of KCl−SiO_2−xanthan NCs. The common salt of this NC is composed of KCl, which is widely used in the oil and gas industries as an additive to drilling fluid and wettability alteration agents in EOR applications. Using SiO_2 as a nanoparticle is common in various industry sectors, such as EOR. Last, xanthan gum is a polysaccharide with a wide range of industrial applications, from the food industry to EOR applications. The required materials for synthesizing the NC include Na_2SiO_3, *Euphorbia condylocarpa* plant extract, xanthan

https://doi.org/10.1021/acsomega.3c05921
ACS Omega 2023, 8, 43930−43954

Table 3. Crude Oil Compositions[a]

component	C_3	iC_4	nC_4	iC_5	nC_5	C_6	C_7	C_8	C_9	C_{10}	C_{11}	C_{12}^+	total
percent	0.11	0.52	1.22	1.30	1.40	8.26	9.72	6.90	7.34	5.26	5.21	52.96	100.0

[a]The specific gravity of residual oil @60.6°F = 0.9211. Oil gravity of residual oil = 22.12° API. Density of total gas evolved = 1.1259 g/L.

Figure 2. AVBP plant (a). AVBP powder (b) used in this study.

Table 4. Physical Properties of the AVBP Powder

test	method	unit	result
appearance	organoleptic		light brown
assay Aloin	HPLC	mg/100 mg	18.700
loss on drying	oven	%	4.600
total ash	furnace	%	11.810
Cu	AA	ppm	1.470
Cd	AA	ppm	0.012

gum, KCl, and ethanol. The pH adjustment was also performed by adding NaOH to the solution. Some of the physical properties of the nanomaterial are shown in Table 5. The characterization of the NC used in this investigation is discussed thoroughly in one of the coauthor's previous works.[40]

Table 5. Properties of the NC Used in This Study

			material composition (wt %)		
nanocomposite composition	particle size	color	carbon	oxygen	silicon
SiO_2/KCl/xanthan gum	28−47 nm	gray	11.61	58.13	30.25

2.1.4. Sandstone Reservoir Rock. The sandstone rock samples used in this study were collected from a sandstone reservoir in southwest Iran. The sampling was carried out from the Asmari Formation of this reservoir. The X-ray diffraction (XRD) analysis of the sandstone sample is shown in Figure 3a, and the images of the actual samples are shown in Figure 3b. The rock sample contains 94.5% quartz, which shows high-quality sandstone. Four core samples with a radius of 3.7 cm (∼1.5 in.) were cut from a whole core drilled from a homogeneous sandstone formation in this reservoir. The sandstone core samples used in this study have an average porosity of 21.63 to 22.63% and an average permeability of 31.82 to 33.45 mD. In addition, the length of these samples was 8.25 to 8.35 cm with a diameter of 3.70 cm. Moreover, the bulk volumes of these samples were 88.70 to 90.42 cm^3. The petrophysical properties of the core samples used in this investigation are shown in Table 6.

2.2. Methodology. The research is subdivided into characterization tests, batch experiments, and dynamic experiments. The characterization experiments aim to understand the characteristics of the AVBP used in this investigation through several analyses such as ^{1}H NMR, TGA, FTIR, UV, and SEM. The chief aim of batch experiments is to understand the mechanisms and interactions of the chemicals used in this study when contacting reservoir rock and fluid. To this end, several IFT, wettability alteration, and rheology tests were conducted to help get a better understanding of the behavior of the fluids when used as CEOR agents. In the next step, the thermal stability, the polymer's absorption, and the polymer's compatibility with reservoir rock and fluids were examined in the presence of salts (stability tests). The last part of the batch experiments was related to investigating the synergistic effects of combining AVBP with ethanol and NC. Finally, dynamic (flooding) experiments were conducted to test the solutions under reservoir conditions, and optimum concentrations of chemicals were proposed. The following sections explain each part of the procedure in more detail.

2.2.1. Characterization Tests. To characterize the polymer, FTIR and ^{1}H NMR techniques are employed to identify the polymer's structures and functional groups. In this study, the FTIR analysis was performed using a Varian (USA) INOVA 500 MHz−125 MHz, in which wavenumbers of 500 to 4000 cm^{-1} were used for scanning the samples. ^{1}H NMR was performed using a Bruker 500 MHz spectrometer. The thermal stability of the polymer is a significant factor for CEOR and is measured using the TGA test. This study used a Q600 (TA Instruments, USA) analyzer with a heating rate of 10 °C/min.

https://doi.org/10.1021/acsomega.3c05921
ACS Omega 2023, 8, 43930−43954

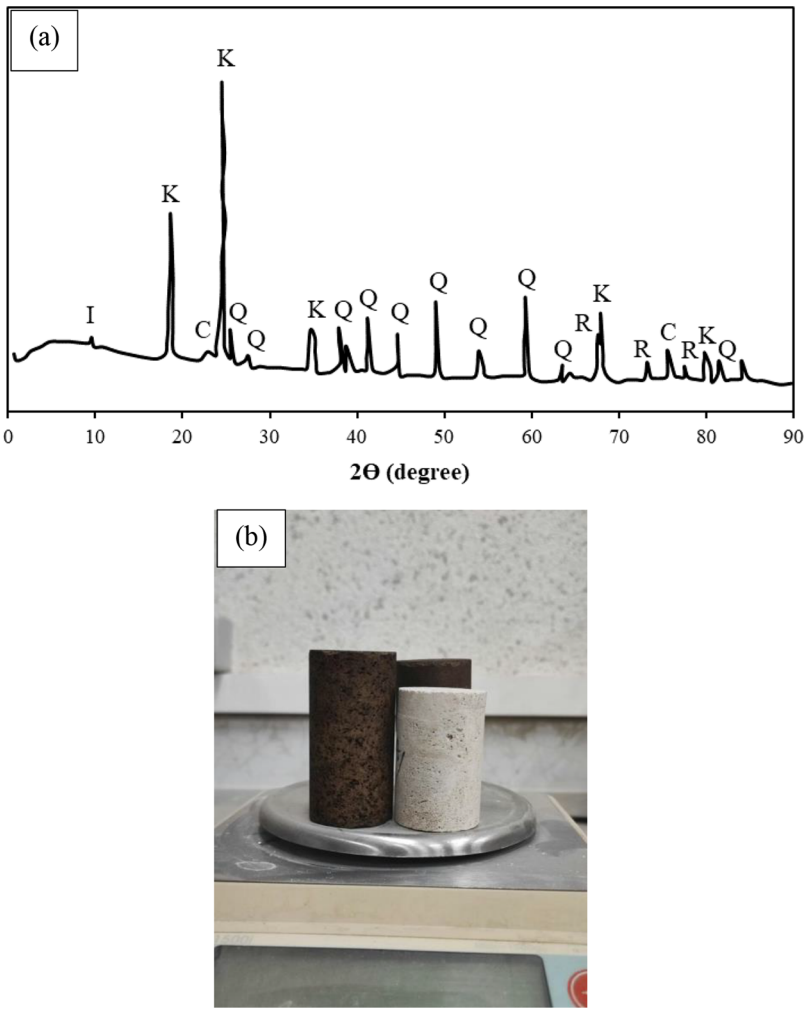

Figure 3. XRD analysis (a) for sandstone sample (b) used in this study (in part a, I stands for illite, K stands for kaolinite, C stands for calcite, Q stands for quartz, R stands for rutile).

Table 6. Properties of Core Samples Used in This Research

no.	length (cm)	diameters (cm)	bulk volume (cm^3)	dry weight (g)	saturated weight (g)	pore volume (cm^3)	porosity (%)	gas permeability (mD)
A	8.35	3.7	89.57	154.15	174.42	20.27	22.63	32.53
B	8.33	3.7	89.56	152.72	172.87	20.15	22.50	31.82
C	8.25	3.7	88.70	150.23	169.95	19.72	22.24	33.45
D	8.41	3.7	90.42	155.46	175.01	19.55	21.63	32.87

The temperature was increased from 25 to 300 °C, and the weight loss was measured accordingly. SEM (TESCAN MIRA II, Czech Republic) is applied to produce high-resolution images that assist in qualitatively analyzing the surface morphology of polymers. Moreover, the viscosity changes of polymer solutions at various shear rates (rheology) were analyzed. Last, to better understand the in situ performance of the polymer, its interactions with reservoir rock (absorption analysis) and FW (compatibility analysis) were studied. In the next series of experiments, ethanol is added to the polymer and the rheological property of the solution is investigated. The IFT of the solution is measured, and wettability alteration is estimated. The NC was added to the previous solutions for the last part of the batch experiments, and various tests, including wettability alteration, viscosity, and IFT experiments, were conducted. As the NC had been characterized and discussed in detail in one of the coauthors' previous works,[40] the characterization section of this study was dedicated to that of the polymer (AVBP).

The sandstone core samples were characterized through porosity, permeability measurement, and XRD analysis. The permeability of the core samples was measured using the gas permeability method using a Coreval 700 instrument (Vinci Technologies). This equipment uses the unsteady-state pressure drop method, and core permeability is measured under different confining pressures of 400 to 10,000 psi. The measured data is collected using a data acquisition and processed using the software. Then, the permeability of each core sample is measured using the unsteady-state pressure drop method. Porosity and pore volume measurements are made using Boyle's and Charles' law techniques. The XRD pattern of the core sample was determined using a D8 Bruker XRD (made by Germany), where 1 g of the sample was inserted into the XRD machine with scanning speed of 1°/min from 5 to

https://doi.org/10.1021/acsomega.3c05921
ACS Omega 2023, 8, 43930−43954

70° under 40 kV/40 mA. The experimental procedure in this section was followed from the literature data.[1,3,7]

2.2.2. Batch (Static) Experiments. 2.2.2.1. IFT and Wettability Alteration Measurements. In this study, to measure the IFT values, the pendant drop method was employed. In this method, a droplet of oil is released into the desired solution and the dimensions of the drop are measured. The IFT is then calculated by using the Young−Laplace equation. Figure 4a shows a typical setup for IFT measurement

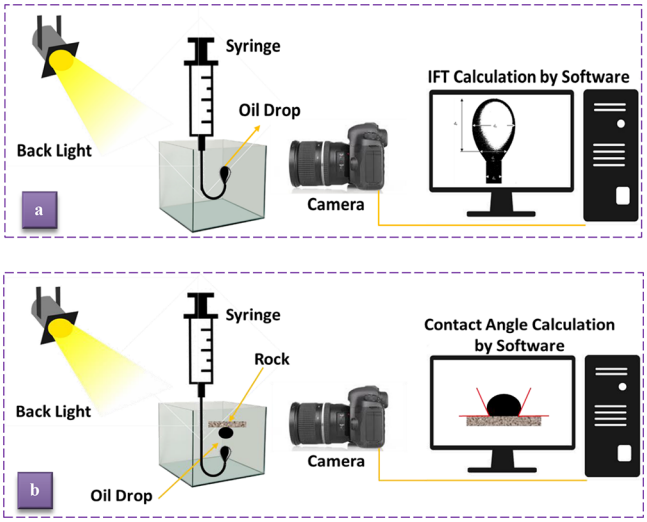

Figure 4. Schematic of the apparatus used in this study for IFT (a) and measurements (b).

using a pendant drop.[41,42] Moreover, the CA measurement method was used to examine the wettability alteration. The apparatus bears many similarities to the IFT measurement. The only difference during the CA measurement is that a thin section is cut from the core samples and then, after cleaning with toluene and DIW, is aged in a reservoir oil (for 30 days to reach the original wettability). Reservoir X is an oil-wet reservoir; hence, to simulate the reservoir conditions in the lab space, the thin section is placed in a chamber and injected with crude oil at a pressure of 1000 and a temperature of 50 °C for 48 h. After the thin sections were aged, the sample was ready for CA measurements. Wettability alteration can be estimated in the presence of crude oil and the desired solutions. For this purpose, the aged thin sections were placed in small glass containers filled with the desired solution at a specified concentration. The samples were then located a short distance from the bottom of the glass container. The crude oil was released from the needle, moved upward, and stuck to the rock's surface. The position of the drop on the rock's surface was tracked and recorded using a high-quality photography system. Three drops were placed on different parts of the thin sections, and then the drop profile was investigated by using drop shape analysis software. The edges of the droplets were tracked, and the equilibrium value of the rock surface was measured (Figure 4b).[23,33,43]

2.2.2.2. Absorption. To study the absorption of various concentrations of polymer solution on reservoir rock, ultraviolet−visible spectroscopy (UV-S) was used in this study. We utilized an Agilent Cary 60 spectrophotometer with a wavelength between 900 and 190 nm to evaluate polymer concentrations (0.5−2.0 g/100 mL) in a static condition. A calibration curve was generated for absorbance-known polymer concentration data, and the polymer concentration was determined using this curve.[44,45] The static absorption test was conducted with 8 g of crushed sandstone core and 40 mL of solution (the polymer to crushed sand ratio was 1:5). The crushed sandstone was sieved with a mesh size of 150−212 μm. The following steps were performed to measure the static absorption test: three concentrations of the desired polymer solution were prepared and combined with crushed sandstone in the previously mentioned ratios. Then, the absorption, which occurs at the maximum wavelength, was plotted versus time for each concentration via a UV device. Eventually, the final absorbance values were determined for each concentration and the maximum wavelength method determined the concentration−absorption reference graph.

2.2.2.3. Compatibility Analysis. The initial equilibrium of the reservoir is disturbed upon application of CEOR. Thus, the compatibility of the injected polymer solution and the FW is crucial. The incompatible polymer solution and FW result in formation damage and plugging of pore throats. We prepared NaCl solutions at various concentrations of 5000, 10,000, 25,000, 50,000, 75,000, 100,000, and 150,000 ppm. The compatibility of AVBP with these solutions and synthetic FW was also investigated. To conduct these tests, 5 mL of various NaCl solutions and 5 mL of polymer solution (with a concentration of 1 g/100 mL) were stirred and poured into the test tube. The test tubes were kept at 25 °C for 14 days. Finally, the precipitations of each test tube were separated by filter paper and placed in the oven for one day. The dried precipitations were carefully weighed and recorded.[46−49]

2.2.2.4. Viscosity and Rheological Properties Measurement. Using a circulating bath (Cole-Parmer Polystat, U.S., and a Peltier AR-G2), the viscous behavior of solutions was studied in steady shear flow at 25 °C. The shear rate was changed in a range of 0.1−300 1/s. Data were adjusted to the Arrhenius equation (eq 1).[50,51]

$$\eta = A^{*}\exp\left[\frac{E_a}{R}\left(\frac{1}{T}\right)\right] \quad (1)$$

where η is the measured viscosity (Pa·s), A *is* the Arrhenius constant, E_a is the activation energy (kJ/mol), and R is the universal gas constant (8.314 kJ/mol·K).

2.2.3. Dynamic (Flooding) Experiments. Core flooding is often used to simulate the movement of fluids under conditions more representative of the reservoir. The procedure started by washing core samples and cleaning them using a Soxhlet apparatus. The samples are then dried in an oven for 24 h. The porosity of the samples was calculated using the saturation method, as summarized in Table 6. The procedure continues by inserting the core plugs into the sample holder. The desired fluids were then injected into the core sample by using high-pressure pumps. A hydraulic jack is utilized to impose overburden pressure on the core sample. Brine was then pumped into the core sample until it was fully saturated. Next, the oil sample was injected into the core to reach irreducible water saturation (Sw_{ir}). After that, the core samples were preserved in a crude oil container at 50 °C for 30 days to make them fully oil-wet. The initial reservoir conditions of the rock samples have been created up to this point. At this stage, different CEOR scenarios can be applied to the core(s) to achieve the optimum outcomes (RF and injection parameters). In addition to the RF, other required parameters, such as

https://doi.org/10.1021/acsomega.3c05921
ACS Omega 2023, 8, 43930−43954

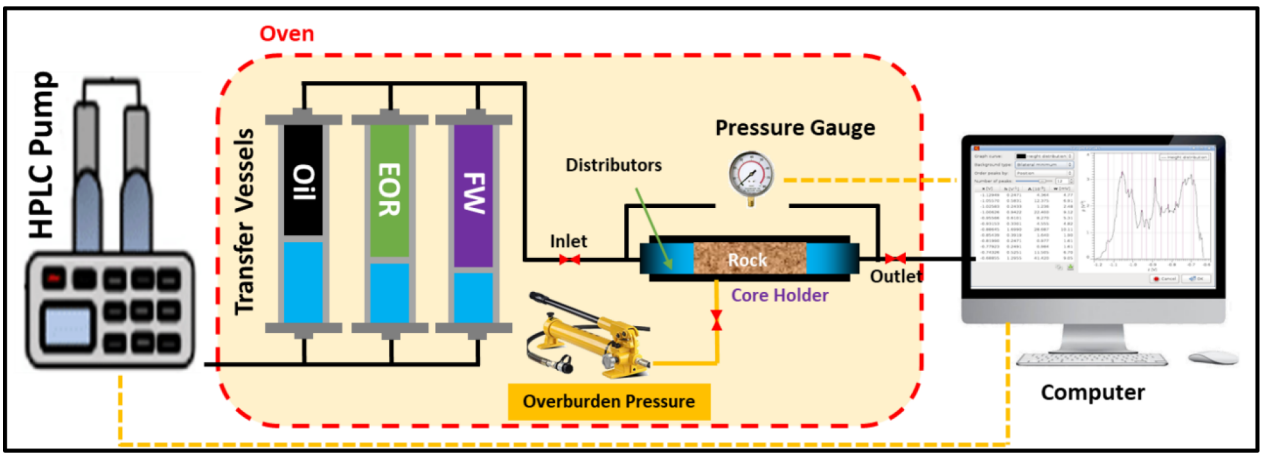

Figure 5. Schematic of the core flooding setup used in this study.

postflooding water saturation (Swc) and relative permeability (Kr) of phases, can be obtained from the flooding test, as well. Figure 5 illustrates a schematic of a flooding apparatus and its various components used in this study.[52−55]

2.2.3.1. Relative Permeability and Fractional Flow Analyses. Steady state and unsteady state are two general approaches for measuring the relative permeability. Although the steady-state methods are highly accurate, they are very time-consuming.[56−59] The unsteady-state approach bears some inaccuracies but is significantly quicker. Therefore, numerous calculations in laboratories, simulators, and even field operations are based on the unsteady-state method. In this study, the *Cory* method was applied for the determination of the relative permeability curves from the following equations:

$$K_{rw} = \alpha \times \frac{(S_W - S_{Wcrit})}{(1 - S_{Wcrit})} - b \times (S_W - S_{Wcrit}) \times \left[\frac{(S_{wc} - S_{orw})}{(1 - S_{Wcrit} - S_{orw})}\right]^2 + c \times \left[\frac{(S_{wc} - S_{Wcrit})}{(1 - S_{Wcrit} - S_{orw})}\right]^4 \quad (2)$$

$$K_{row} = d \times \frac{(S_o - S_{orw})}{(1 - S_{orw})} \times \left[\frac{(S_o - S_{orw})}{(1 - S_{wcon} - S_{orw})}\right]^2 \quad (3)$$

where K_{rw} and K_{row} are the relative permeability of water and oil phases, water and oil saturation are represented by S_W and S_o, respectively, S_{wcrit} stands for critical water saturation, S_{orw}represents the residual oil saturation post water flooding, and S_{wcon} indicates connate water saturation. The coefficients $a-d$ change for various complexities of the crude oil, brine, and rock conditions. Fractional flow analysis is a robust tool used primarily in water-based EOR operations. It helps identify the underlying mechanisms of the CEOR process, explains the fluid behavior in porous media during the process, and is a validation tool for reservoir simulators. The fractional flow analysis can be calculated as follows:

$$f_w = \frac{1}{1 + \frac{k_{ro}}{\mu_o}\frac{\mu_w}{k_{rw}}} \quad (4)$$

where k_{ro} and k_{ro} are the relative permeability of water and oil phases, and the viscosity of oil and water are shown by μ_o and μ_w, respectively. In addition, the capillary numbers and mobility ratios for the solutions are calculated using the following equations:

$$N_{Ca} = \frac{v\mu}{\sigma} \quad (5)$$

$$M = \frac{k_{rD}}{K_{rd}} \times \frac{\mu_d}{\mu_D} \quad (6)$$

where N_{Ca} is the dimensionless capillary, v is the velocity in cm/s, μ is the viscosity of the displacing (in our case, CEOR) agent in cp, σ is IFT between oil and CEOR agents in dynes/cm^2, $\frac{k_{rD}}{K_{rd}}$ is the ratio of the relative permeability of CEOR agent to that of oil, and $\frac{\mu_d}{\mu_D}$ is the ratio of the viscosity of oil to that of CEOR agent. Using N_{Ca} and M can shed some light on the microscopic (displacement efficiency) and macroscopic (volumetric sweep efficiency) performance of CEOR agents in porous media. This can result in an in-depth understanding of the underlying mechanisms of the CEOR agent and ultimately improve the efficiency of the process.

3. RESULTS AND DISCUSSION

3.1. Characterization of AVBP. *3.1.1. FTIR and ^{1}HNMR analyses.* FTIR and ^{1}HNMR analyses were conducted to identify the polymer's structures and functional groups, as shown in Figures 6 and 7. FTIR was performed in the wavelength range of 400 to 4000 cm^{-1}, as seen in Table 7.

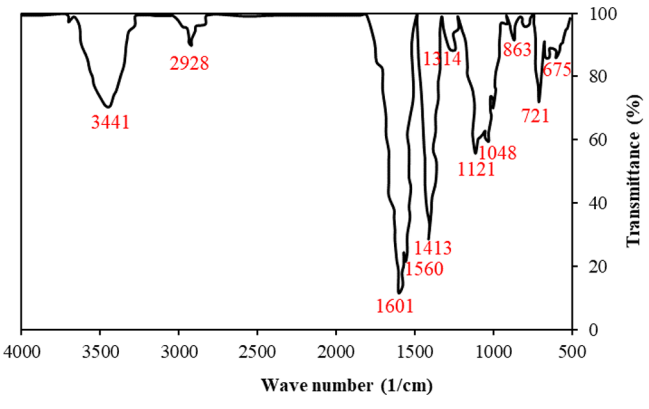

Figure 6. FTIR analysis of AVBP.

https://doi.org/10.1021/acsomega.3c05921
ACS Omega 2023, 8, 43930−43954

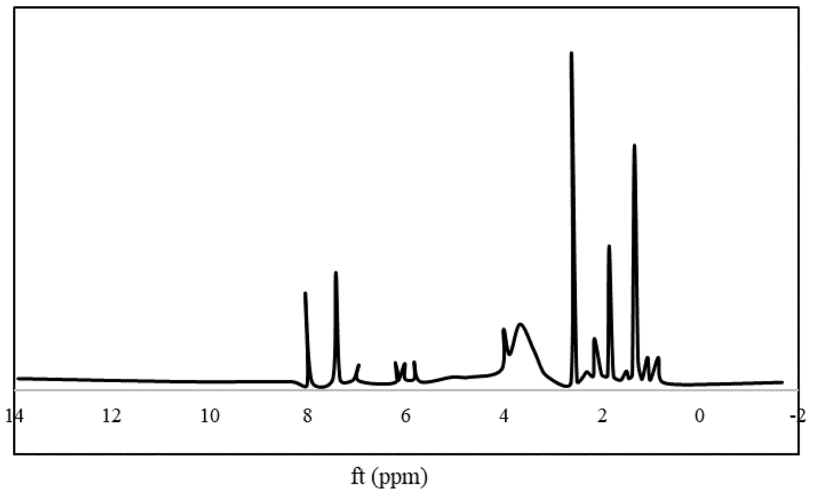

Figure 7. ^{1}H NMR analysis of AVBP.

Table 7. FTIR Functional Group Peaks

wavenumber (cm^{-1})	functional group	vibration mode	compound class
3444.41	O−H	stretching	alcohol
2928.15	C−H	stretching	alkane
1601.34	N−H	bending	amine
1560.40	N−O	stretching	nitro compound
1413.21	C−H	bending	alkane
1314.68	O−H	bending	phenol
1264.94	C−O	stretching	alkyl aryl ether
1121.28	C−O	stretching	secondary alcohol
1048.14	S═O	stretching	sulfoxide
863.57	C−H	bending	1,2,4-trisubstituted
776.36	C−H	bending	1,2-disubstituted
721.30	C−H	bending	1,3-disubstituted

Wavelengths between 1000 and 1200 cm^{-1} proved that the AVBP contains glycoside (a polysaccharide structure). The β- and α-configurations of the polysaccharide can be detected from the peaks ranging between 810 and 881 cm^{-1}. Pyranose (sugar) can be attributed to a peak occurring at 1075.06 cm^{-1}. Different components such as malic acid, polysaccharide acemannan, glucose, and the three main natural components of AVBP can be detected from the typical NMR spectrum. Acemannan is a β-(1−4)-linked mannan partially acetylated in position 2, 3, or 6. The outcomes of this section are in good agreement with the literature data.[51,60,61]

A characteristic signal (2.00 and 2.26 ppm) created by acetyl groups within the ^{1}H NMR spectrum can be identified as the AVBP fingerprint. However, there is a small amount of acemannan and malic acid due to the low signal of the NMR spectrum. The signal at 5.4 ppm shows a considerable amount of maltodextrin in the sample. Different organic acids can also be detected from the NMR spectrum. Lactic acid is seen to be 1.33 ppm. Acetic and succinic acids were observed in a large amount of AVBP. Lactic acid is not a natural ingredient of the AVBP; instead, it is the final product of *Lactobacillus* fermentation. Thus, the presence of a significant amount of lactic acid reduces the quality of raw materials. Enzymes may produce succinic acid, fumaric acid, and pyruvates during the citric acid cycle. Therefore, some enzymes create organic acids within the gel if a suitable thermal manipulation is not quickly performed. The achieved data in this section agree with the literature data.[62,63]

3.1.2. Thermal Stability Analysis (TGA Curve). Figure 8 shows the thermal analysis used to evaluate the temperature stability of the polymer. We used 0.67 mg of the sample to perform the test. Argon gas, at a rate of 10 cc/min, was used to

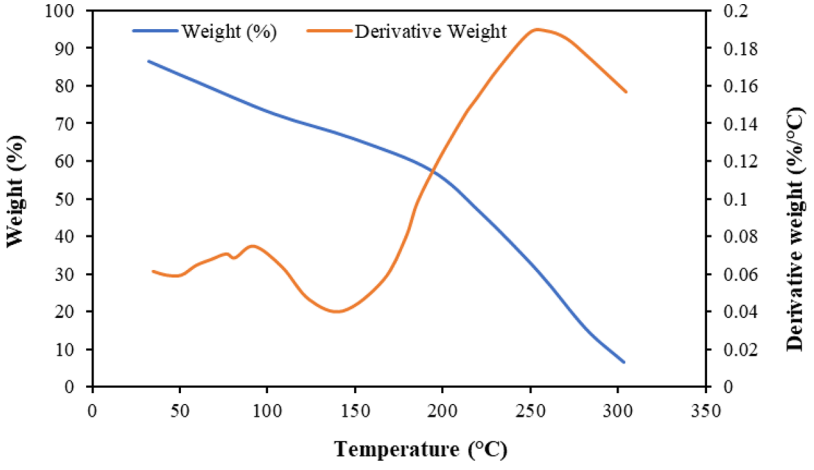

Figure 8. TGA test of AVBP.

https://doi.org/10.1021/acsomega.3c05921
ACS Omega 2023, 8, 43930−43954

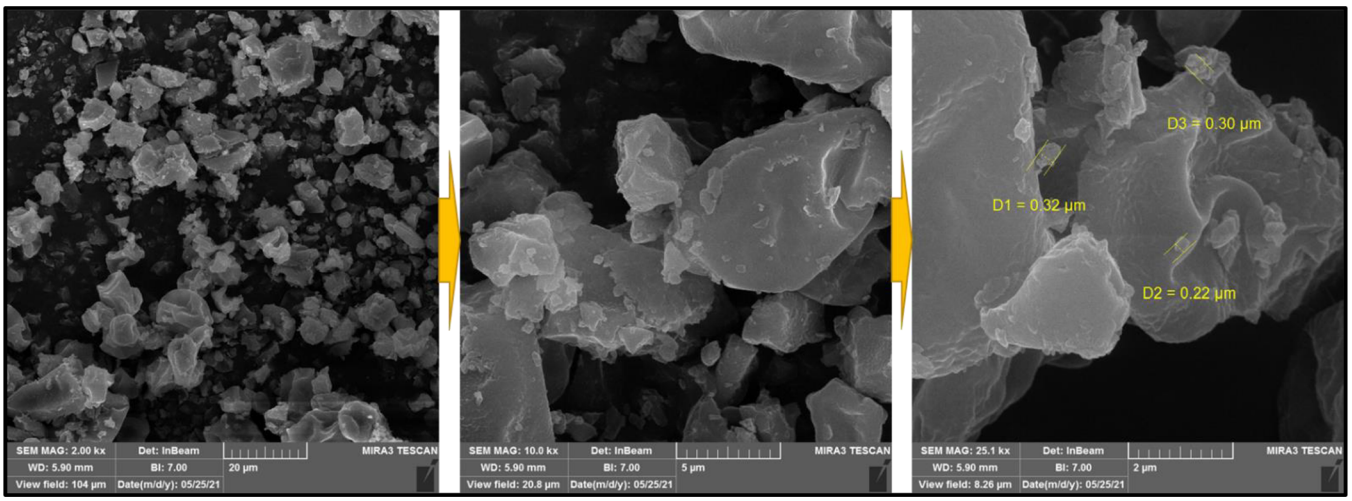

Figure 9. SEM analysis for AVBP.

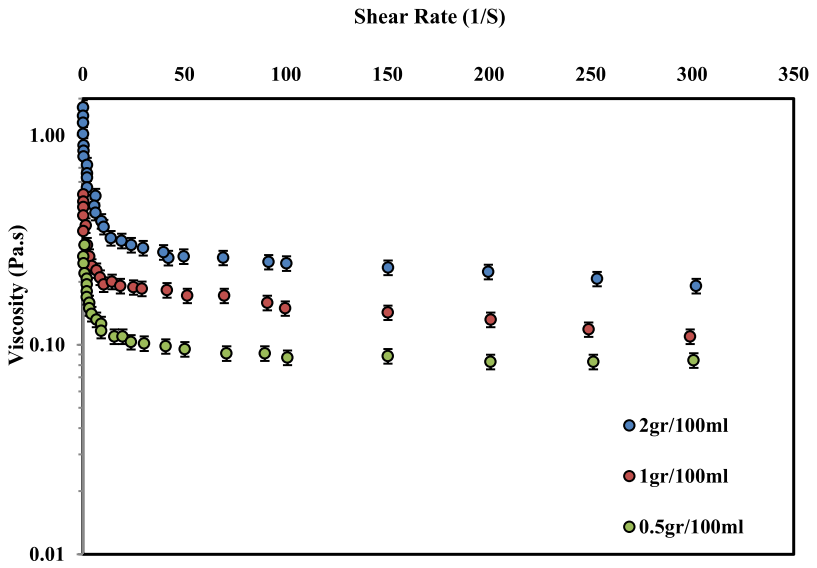

Figure 10. Viscosity of AVBP versus the shear rate at different concentrations.

increase the temperature during the experiment. As shown in this figure, for the temperature range of 25 to 300 °C, the polymer lost about 28.11% of its initial volume, which is considered acceptable for polymers that do not have relatively high-temperature stability. At a temperature of 94.40 °C, about 3.92% weight loss was observed. It should be noted that reservoir X has normal temperature gradients; hence, at the hydrocarbon-bearing zone, the temperature does not exceed 90 °C. Therefore, the polymer used in this study is expected to be thermally stable in the reservoirs with normal temperature gradients. Weight losses at temperatures above 100 °C can also be attributed to surface moisture and structural water evaporation. The achieved data in this section agree with the literature data.[64,65]

3.1.3. Powder Particle Morphology (SEM Analysis). The surface morphology of AVBP is investigated using SEM at magnifications in the range 2−20 μm, as shown in Figure 9. The particle sizes of this substance are in the range of microns, which indicates that they are suitable chemicals for injection into reservoirs. It can also be observed that the particles have spherical structures. The spherical nature of the particles shows that the droplets have dried uniformly during the drying process. The achieved data in this section agrees with the literature data.[65−67]

3.2. Batch Experiments. *3.2.1. Rheological Properties of AVBP Solutions. 3.2.1.1. Rheology of AVBP.* This section measured the viscosity of the solution (Pa·s) at different shear rates (1/s) for three different concentrations. Figure 10 illustrates the viscosity versus the shear rate for each concentration. The viscosity was measured for shear rates between 1 and 300 1/s. It is evident from the figure that this substance has an entirely Newtonian behavior. Therefore, it will be suitable for injection into the reservoir as a CEOR agent. Furthermore, in steady-state conditions, the viscosity for this material is between 0.09 and 0.19 Pa·s (90 and 190 cP), which is considered suitable from an injectivity point of view without putting a strain on the injection pumps. Higgs and Wang (2023) state that incremental oil recovery is more significant when the polymer viscosity increases. In addition, as presented in eq 6, increasing the polymer's viscosity directly affects reducing the M value, where lower values of M are achieved. Therefore, it is expected to perform better with 2 g of polymer than with 0.5 g of polymer in solution. Hence, the resulting M value is lower in the case of a 2 g polymer.

https://doi.org/10.1021/acsomega.3c05921
ACS Omega 2023, 8, 43930−43954

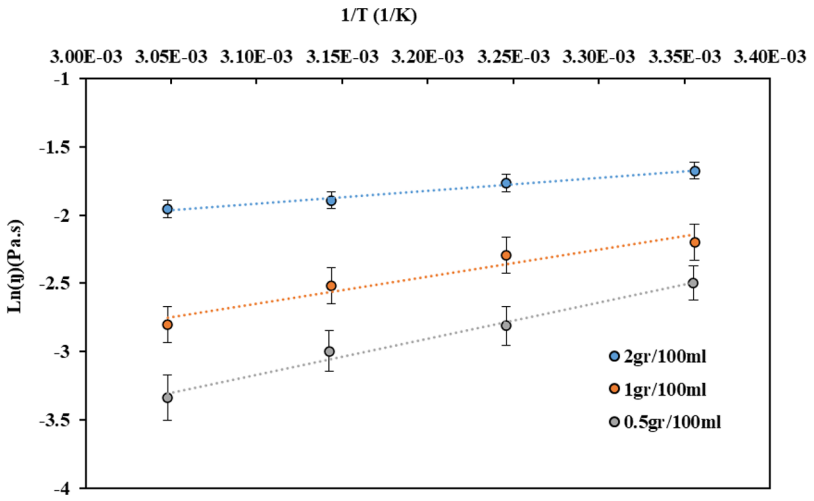

Figure 11. Effect of temperature on viscosity for AVBP at different concentrations.

Consequently, the expected RF and sweep efficiency would be higher than the solution with 0.5 g of polymer. The experimental achievements in this study agree with the literature data.[68−70]

The Effects of Temperature on Rheology of AVBP: Temperature is another critical parameter that affects the rheological properties of the polymeric materials. The viscosity of the solution was measured as temperatures elevated from 298 to 328 K, as shown in Figure 11. The Arrhenius equation was used to calculate the temperature dependence of the reaction rates. Overall, the viscosity of the AVBP solution decreased as the temperature rose. The values of the parameters required to analyze the effect of temperature have been measured and are given in Table 8. The activation

Table 8. Arrhenius Equation Parameters for AVBP.

concentration	A (Pa·s)	E_a (kJ/mol)	R^2
2 g/100 mL	0.002800	122.781	0.9916
1 g/100 mL	0.000148	238.646	0.9443
0.5 g/100 mL	0.000008	325.884	0.9844

energy (E_a) was in the range of 122 to 325 kJ/mol range. The regression coefficient for this model (R^2) was measured to be over 0.98, indicating the high accuracy of this sample's calculated parameters. It could be seen that E_a was reduced as the concentration increased. The low E_a may show a high entanglement configuration and interactions between the polysaccharides in fresh Aloe Vera mucilage, specifically pectins and acemannan. The experimental achievements in this study are in good agreement with the literature data.[70−72]

3.2.1.2. Rheological Properties of AVBP-Ethanol. Testing the rheological properties of the polymers, specifically, the biopolymers, is crucial before field applications. Therefore, the rheology of different polymer−ethanol solutions is investigated in this section, as shown in Figure 12. All the answers exhibited Newtonian fluid behavior. The viscosity was reduced for all solutions as the shear rate increased. The effects of shear rate were more pronounced at higher ethanol concentrations, i.e., 15−20%.

3.2.1.3. Rheological Models. The experimental study of the rheology of a polymer solution showed that the answer follows Newtonian flow behavior. In this section, three standard models, namely, the power law, Herschel−Bulkley, and Cross model, were used to estimate the viscosity of the solution. The two latter models are modifications of the power-law model. A detailed discussion of the differences and backgrounds of the models can be found in the literature. The three viscosity models were applied to calculate the viscosity of the polymer at various concentrations, as shown in Figure 13. The Herschel−Bulkley model (Figure 13a), an improved version of the power-law model, has shown the best results among the presented models. The Herschel−Bulkley model gives a better data regression than the other two, implying that the model must consider a limiting parameter that sets the viscosity to a finite value at zero shear rates. The viscosity prediction using all three models is very close, except for the power-law model at 0.5 g/100 mL, for which the predicted viscosity is slightly more accurate than others. The experimental achievements in this study are in good agreement with the literature data.[44,68,70,73]

In the next part, the previous rheological models were applied to 1 g/100 mL of AVBP containing different concentrations of ethanol (0−20%), as shown in Figure 14a−c. The performance of the models above was almost identical. However, the Herschel−Bulkley model performed slightly better than the others.

3.2.2. AVBP Absorption. Polymer absorption on the rock surface is another crucial issue affecting the technical and economic aspects of CEOR operations and, hence, needs to be carefully studied. Higher absorption means more loss of the polymer and, finally, a higher cost of the operation. The UV device measured the polymer absorption. First, three solutions with the desired concentrations were placed in the device chamber. Figure 15 exhibits the measured UV spectra for polymer solutions with concentrations of 0.5−2 g/100, measured between 200 and 900 nm over a period of 0−120 h. For the polymer solution used in this study, the maximum absorption was observed at wavelengths of 330 nm. The λ_{max} is identical for all of the solutions. According to these diagrams, the absorption at the maximum wavelength is proportional to the absorption of the solution. Therefore, the absorption can be calculated for each concentration at different times (0−120 h).

Figure 16 shows the absorption versus time. It can be seen in the figure that the absorption decreases sharply in the early hours and reduces with a smaller slope approximately 24 h

https://doi.org/10.1021/acsomega.3c05921
ACS Omega 2023, 8, 43930−43954

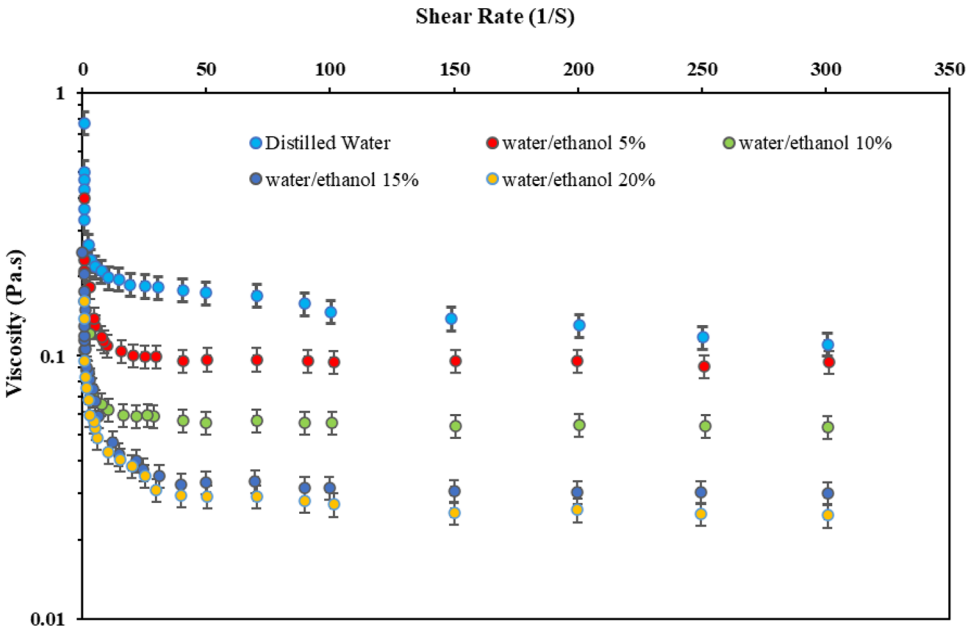

Figure 12. Relationship between viscosity and shear rate for AVBP (1 g/100 mL) at different solvent fractions.

after the test. It was also observed that a higher absorption could be observed in solutions with higher concentrations. For instance, at 0 h, the absorption is approximately 2.9, 3.2, and 3.3 au for 0.5, 1, and 2 g/100 mL, respectively. A similar trend can be observed for the rest of the periods; the equilibrium reached 120 h. The absorption for 0.5, 1, and 2 g/100 mL concentrations was measured to be 2.2, 2.4, and 2.8 a.u, respectively. The absorptions were more significant between the concentration of 1 and 2 g/100 mL, in contrast to 0.5 and 1 g/100 mL. The experimental achievements in this study are in good agreement with the literature data.[74−77]

3.2.3. Compatibility Analysis. The salinity of the FW is often high in hydrocarbon reservoirs. Chemicals, specifically polymers, are sensitive to the salt content and tend to deteriorate as salinity increases. Therefore, the compatibility of polymer solutions and salts must be investigated for a successful chemical injection project. In this part, we first prepared polymer solutions with concentrations of 0.5−2 g/100 mL using DIW, and the solution was left for 14 days. AVBP, which is a biopolymer, is entirely soluble in DIW. As a result, no sediments (precipitates) were formed when the solution was mixed with DIW, as shown in Figure 17a. In the next step, a compatibility test was performed using 1 g/100 mL of polymer in FW and different NaCl concentrations (with salinities ranging from 10,000 to 180,000 ppm), as shown in Figure 17b. For each combination, the formation of sediments was measured. Figure 17b shows that no sediment was formed at brines with salinities below 100,000 ppm. The formation of sediments at the concentration of 130,000 ppm of NaCl and FW (with a salinity of over 175,000 ppm) was 0.132 and 0.187 g, respectively. AVBP solution is compatible with FW based on the quantity of precipitation collected. However, when AVBP solutions are used for CEOR formations with noticeably higher salinities, care should be taken.

3.2.4. IFT Measurements. IFT and wettability are crucial parameters in the success of the CEOR projects. Polymers alone cannot reduce the IFT value or alter the wettability of rocks to increase oil production. On the other hand, alcohols and NC materials are considered effective chemicals for reducing IFT values between fluids for CEOR applications. This section investigates the IFT values of AVBP, AVBP−ethanol, and AVBP−ethanol−NC solutions as CEOR agents.

3.2.4.1. IFT Measurements of AVBP Solutions. First, the IFT between crude oil and polymer solutions versus time was investigated, as shown in Figure 18. The IFT of the polymer solution for concentrations of 0.5, 1, and 2 g/100 mL was 28.2, 24.5, and 22.4 mN/m, respectively. Compared to the reference IFT (the IFT between DIW and crude oil = 32.1 mN/m), IFT reduction when the polymer enters into the system for concentrations of 0.5, 1, and 2 g/100 mL is 12.15, 23.68, and 30.22%, respectively. Although the polymer slightly reduces IFT, it is insufficient to mobilize trapped oil and increase the recovery.

3.2.4.2. IFT Measurements of AVBP−Ethanol Solutions. The addition of other agents such as alcohol or surfactants is common because polymers alone are unable to affect the IFT value in a way that helps improve recovery. For this purpose, in this study, an additive from the alcohol group (ethanol) was used to improve the situation. Ethanol solvent was used in volume ratios of 5, 10, 15, and 20%, and the IFT value was measured as illustrated in Figure 19. As can be seen from the figure, higher ethanol concentrations resulted in lower IFT values. IFT reduction was initially rapid; however, as the ethanol concentration reached 10%, the rate of IFT reduction decreased. The ethanol structure has a hydrophilic head and a hydrophobic end. As a result, it acts as a surfactant, reducing the IFT by creating a bridge between the two phases. As illustrated in Figure 19, for polymer solutions containing ethanol solvent with concentrations of 0, 0.5, 1, and 2 g/100 mL, the IFT values were reduced to 18.5, 16.4, 14.5, and 12.9 mN/m from initial values of 32.1, 28.2, 24.5, and 22.4 mN/m, respectively. In contrast to the benchmark (IFT of oil and DIW), the IFT for the concentrations of 0.5, 1, and 2 gr/100 mL was reduced by 41.85, 40.82, and 42.42%, respectively. It is apparent from the graph that IFT was not changed significantly for the ethanol with a volume percentage of higher than 10%. For a solution with 20% of ethanol concentration, the IFT for polymer concentrations of 0, 0.5, 1, and 2 g/100 mL reduced

https://doi.org/10.1021/acsomega.3c05921
ACS Omega 2023, 8, 43930−43954

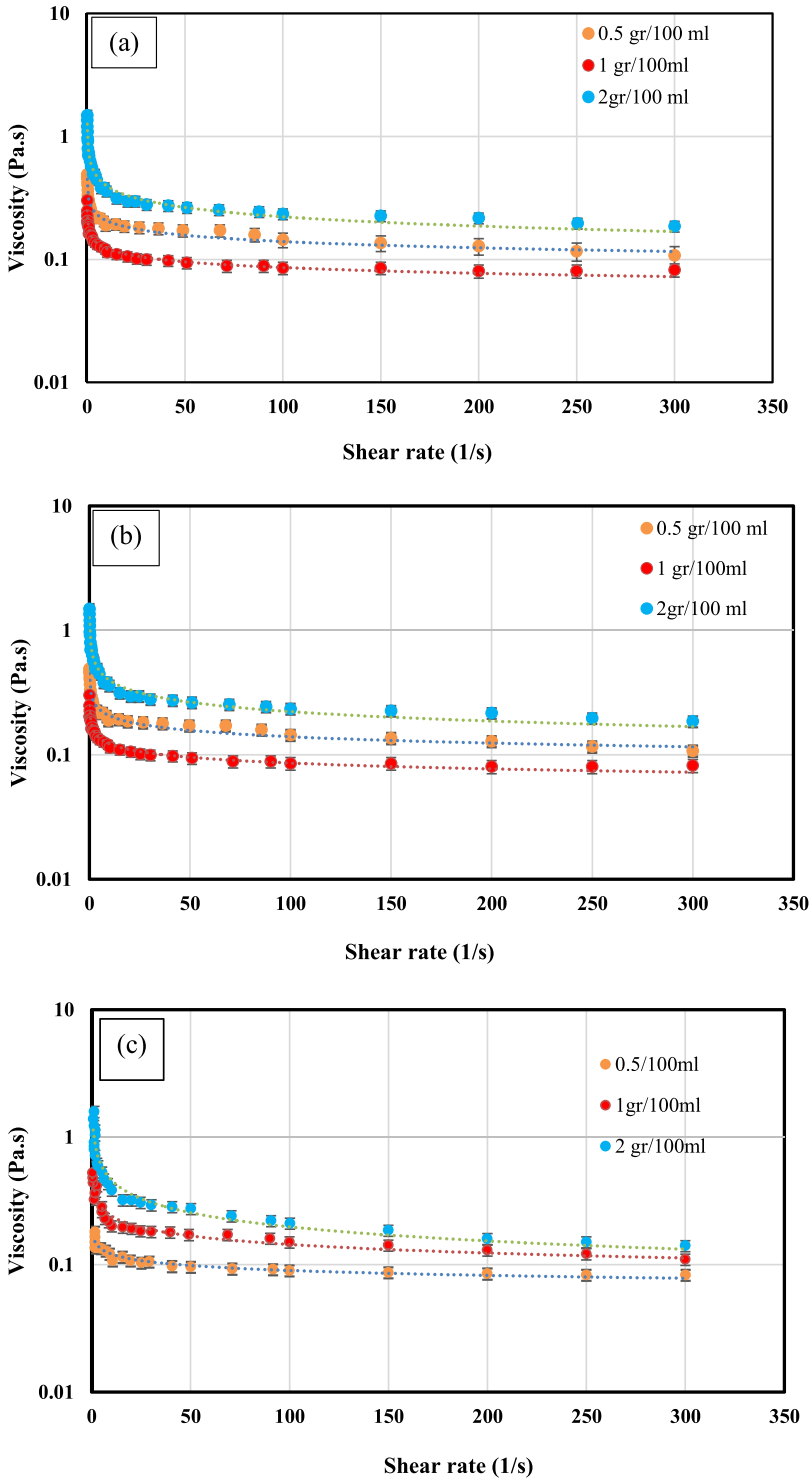

Figure 13. Relationship between the viscosity of AVBP versus shear rate using (a) the power-law model, (b) the Herschel−Bulkley model, and (c) the Cross model at various concentrations.

to 18.5, 16.4, 14.5, and 12.9 mN/m from initial values of 20.5, 17.5, 15.3, and 13.7 mN/m, respectively. The experimental achievements in this study are in good agreement with the literature data.[1,3,7]

The Effects of Temperature on IFT Measurements: Temperature plays a vital role in controlling the IFT of polymer solutions. Figure 20 shows the changes in the IFT values at different ethanol concentrations and various temperatures. It can be observed that at a constant concentration of 1 g/100 mL, the IFT reduces as the temperature increases. Moreover, it can be seen that the effect of ethanol in the system decreased at higher temperatures. This means that at temperatures close to ambient, adding ethanol solvent reduces the IFT values considerably. However, at higher temperatures, the slope of IFT reduction is reduced. Moreover, it was observed that the addition of more ethanol concentrations resulted in lower IFT values, regardless of the temperature. Therefore, both high ethanol concentrations and higher

https://doi.org/10.1021/acsomega.3c05921
ACS Omega 2023, 8, 43930−43954

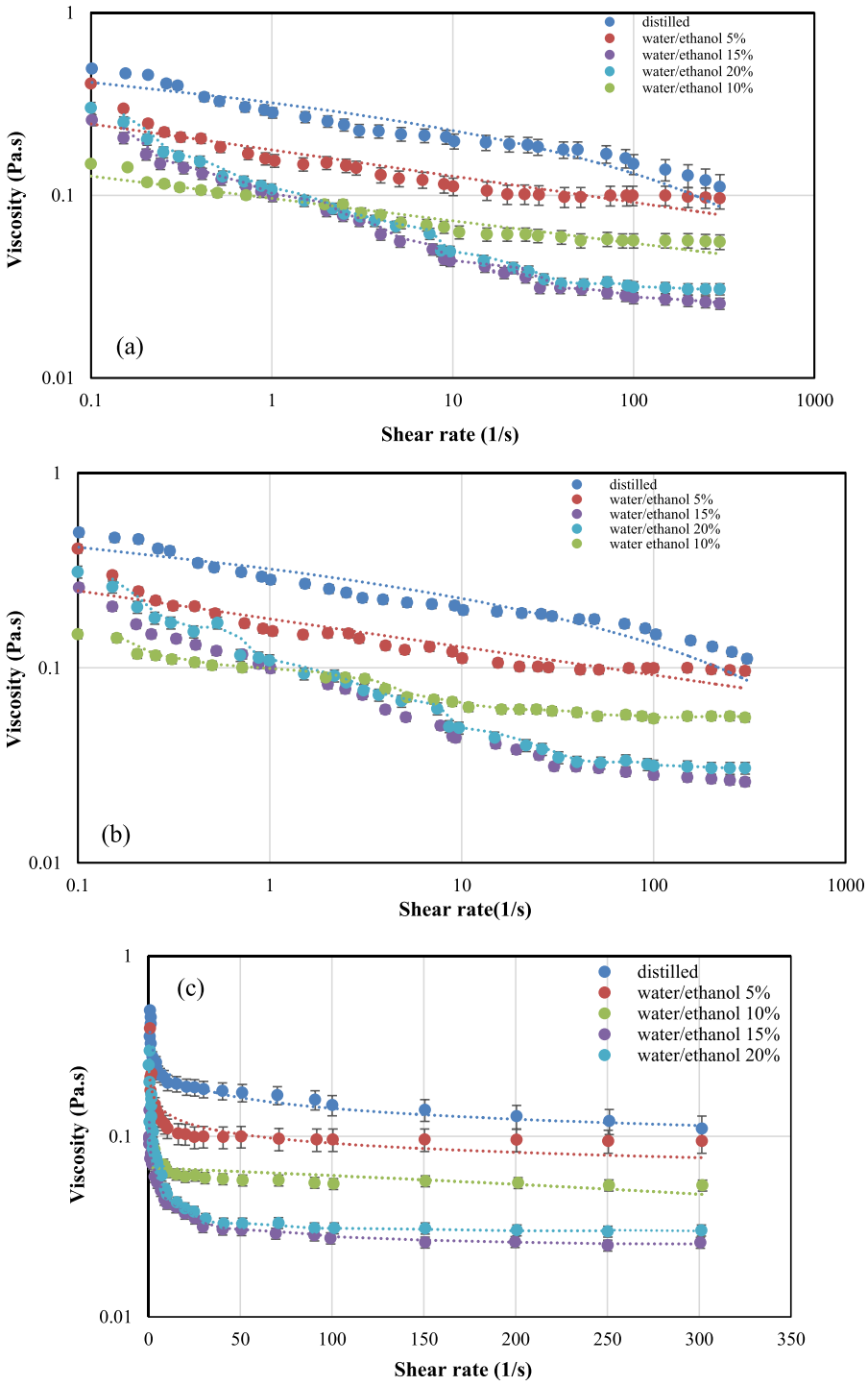

Figure 14. Relationship between viscosity and shear rate using (a) the power-law model, (b) the Herschel−Bulkley model, and (c) the Cross model for AVBP (1 g/100 mL) at different ethanol fractions.

temperatures favor the process from the point of view of IFT reduction. It is believed that increasing the temperature results in reduced free energy between the crude oil and the solution. Thus, the mobility of the water phase and crude oil is increased. In addition, increasing the temperature decreases the intermolecular forces at the interface of the water and oil phases. Hence, the IFT values are reduced with increasing the temperature.[4,78]

3.2.4.3. IFT Measurements of AVBP−Ethanol−NC Solutions. This section investigates the effect of adding NC to the AVBP−ethanol solution. Figure 21 shows the IFT values versus NC concentration for various ethanol solutions at a constant 1 g/100 mL polymer concentration. Moreover, the figure also represents different volume percentages of ethanol solvent. It can be observed that for all solutions, as the concentration of NC increases, the IFT value decreases. The NCs, due to their size, tend to go to the surface between two liquids in the solution and reduce the IFT value of the system. Therefore, adding NCs to the system reduced the IFT values, where the IFT decreased rapidly with an increase in the

https://doi.org/10.1021/acsomega.3c05921
ACS Omega 2023, 8, 43930−43954

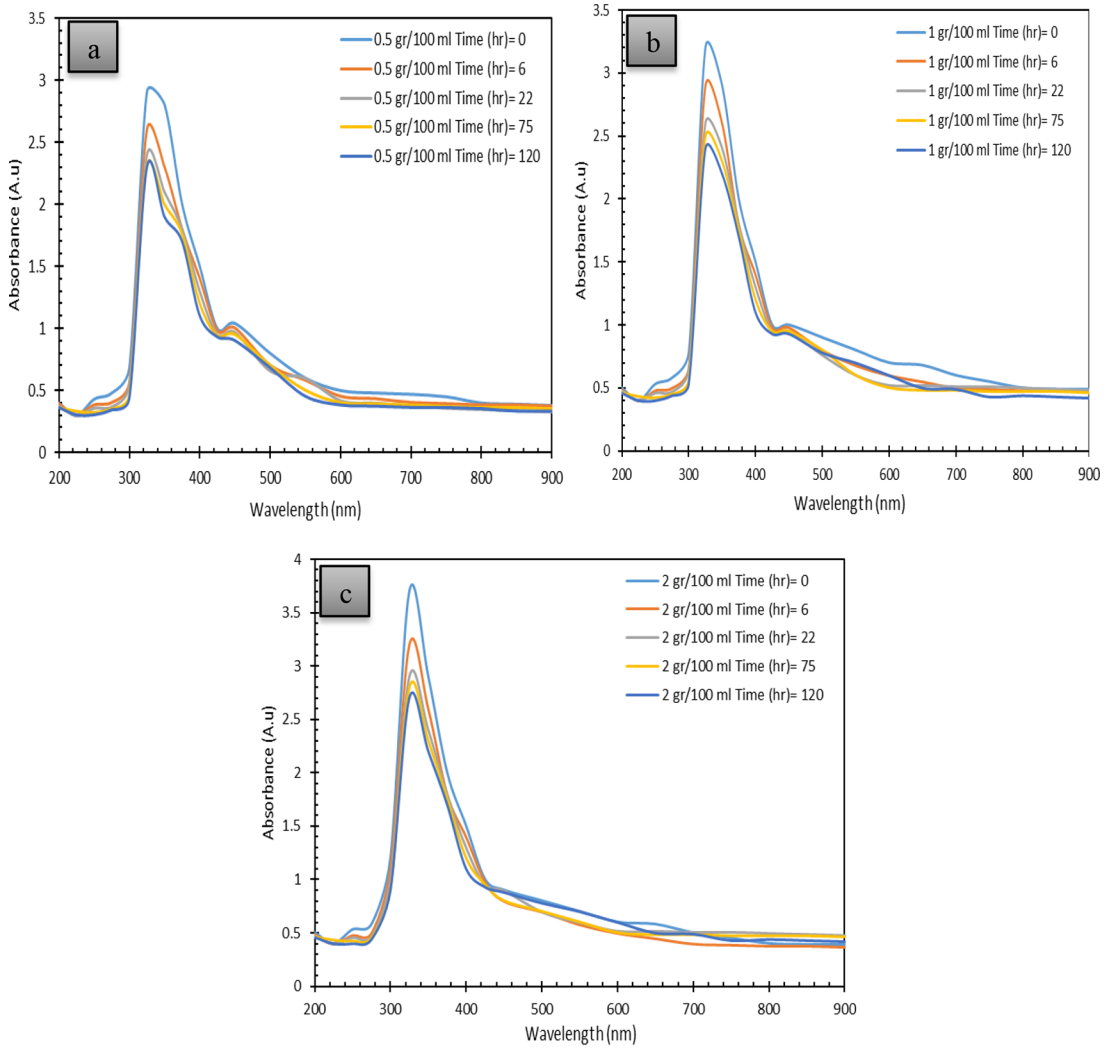

Figure 15. UV−vis absorbance spectra of AVBP solutions in the sandstone core samples at different times for concentrations of (a) 0.5, (b) 1, and (c) 2 gr/100 mL.

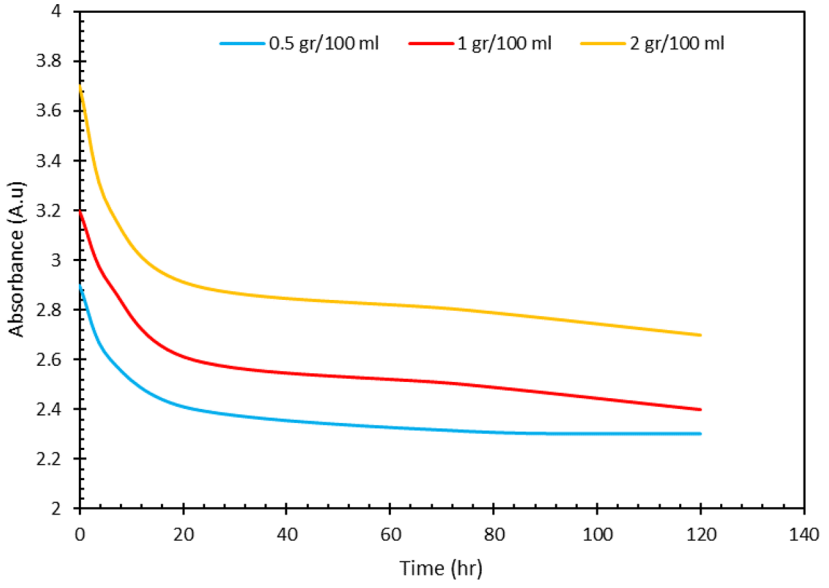

Figure 16. Absorbance reduction of AVBP solutions with the sandstone cores versus time.

https://doi.org/10.1021/acsomega.3c05921
ACS Omega 2023, 8, 43930−43954

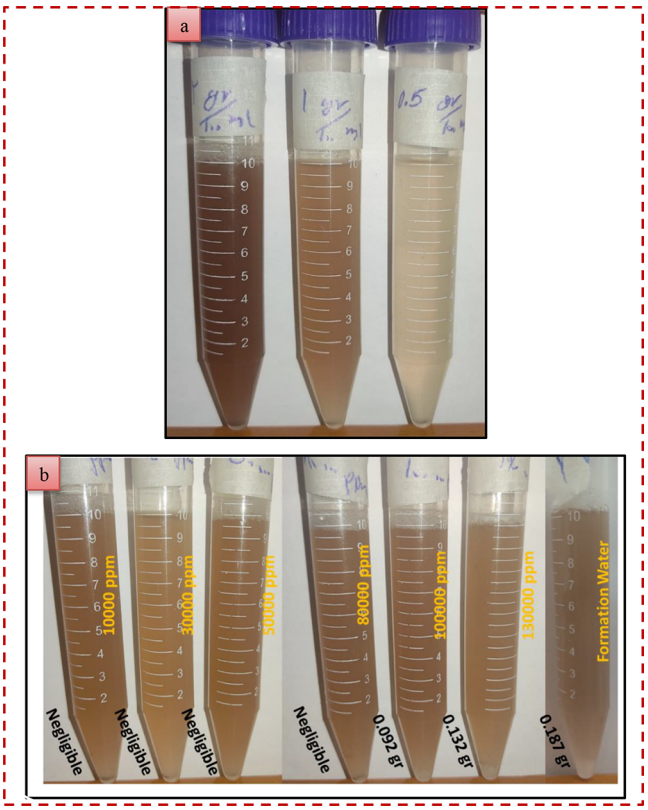

Figure 17. AVBP at different concentrations in DIW (a). Compatibility analysis for 1 g/100 mL of AVBP to varying concentrations of NaCl and FW solutions (b).

concentration of NC. However, once the concentration exceeded 300 ppm, the slope of IFT reduction diminished.

Comparing the results at different volumes of ethanol shows that volume ratios of 5 and 10% significantly decrease the IFT value compared to DIW. It can also be seen that after 10% by volume of ethanol, increasing the ethanol concentration in the system had an insignificant effect on the IFT value. When the concentration of the NC is elevated to 300 ppm, the IFT values of 15, 8.8, 4, 2.2, and 1.7 mN/m were achieved for DIW, 5%, 10%, 15%, and 20% volumes of ethanol, respectively. Therefore, the optimum results can be achieved by selecting a concentration of 300 ppm of NC and 10% ethanol solvent in the prepared solution. Increasing the concentration of ethanol and NC beyond these optimum concentrations makes the reduction of the IFT value insignificant.

3.2.5. Wettability Alteration Measurements (Method). 3.2.5.1. CA Measurements of AVBP–Ethanol Solutions. Wettability is one of the petrophysical parameters that directly and indirectly affect recovery. In this section, the wettability measurement is determined by using the CA method. Figure 22 presents the CA values for the polymer solutions containing different volume percentages of the ethanol solvent. It can be seen in the figure that increasing the volume percentage of ethanol in the system decreased the CA values. The reduction in CA value occurred with a greater slope for volume percentages below 10% of ethanol solvent. For volumes above 10%, as the volume percentage of ethanol was increased, the CA decreased with a smaller slope. For concentrations of 0, 0.5, 1, and 2 g/100 mL of the polymer solutions, the CA decreased from initial values of 168, 150, 130, and 123° to 116, 112, 103, and 100°, respectively. Adding ethanol to the system shifted the CAs from a strongly oil-wet state to a slightly water-wet state. The CA improvements of 30.98, 13.34, 20.77, and 18.70% were observed (compared to the case without ethanol in the system) for concentrations of 0, 0.5, 1, and 2 g/100 mL, respectively. It is believed that increasing the solvent concentration increases the active molecules present in the solution; therefore, the ability of the solution to act in changing the wettability of the rock surface is increased, resulting in more water-wet states at higher solvent concentrations.[4,78,79]

3.2.5.2. The Effects of Temperature on CA Measurements. The effect of temperature on the CA measurements for the polymer solution at a constant concentration of 1 g/100 mL was also investigated in this section. Figure 23 shows the CAs

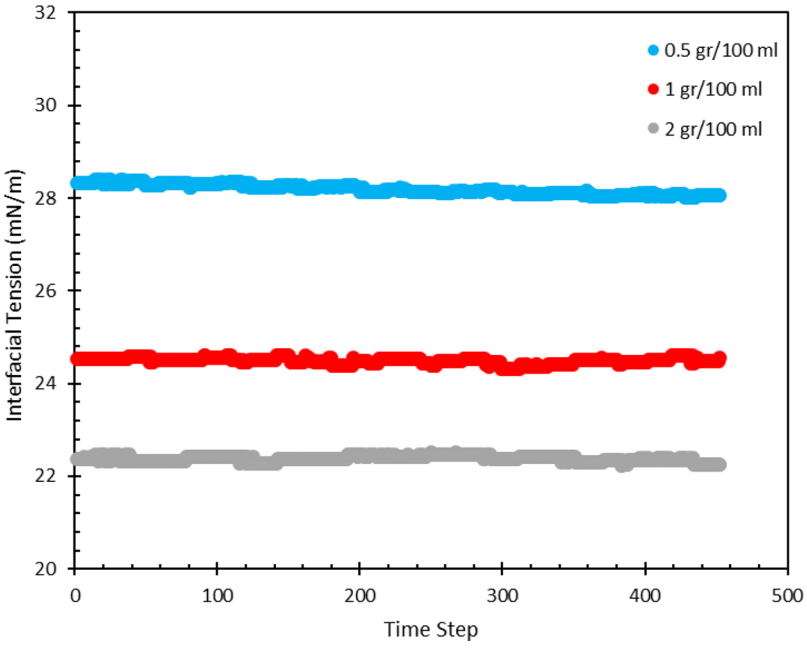

Figure 18. Dynamic IFT measurements for the AVBP solution at different concentrations versus time.

https://doi.org/10.1021/acsomega.3c05921
ACS Omega 2023, 8, 43930−43954

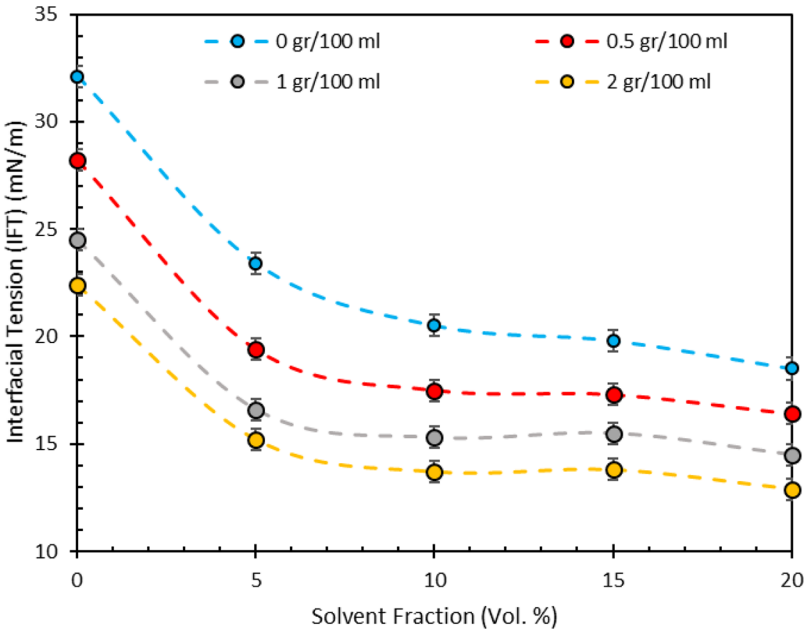

Figure 19. IFT values for different AVBP solutions versus ethanol solvent at various concentrations at P = 14.7 psi, T = 298.15 °K.

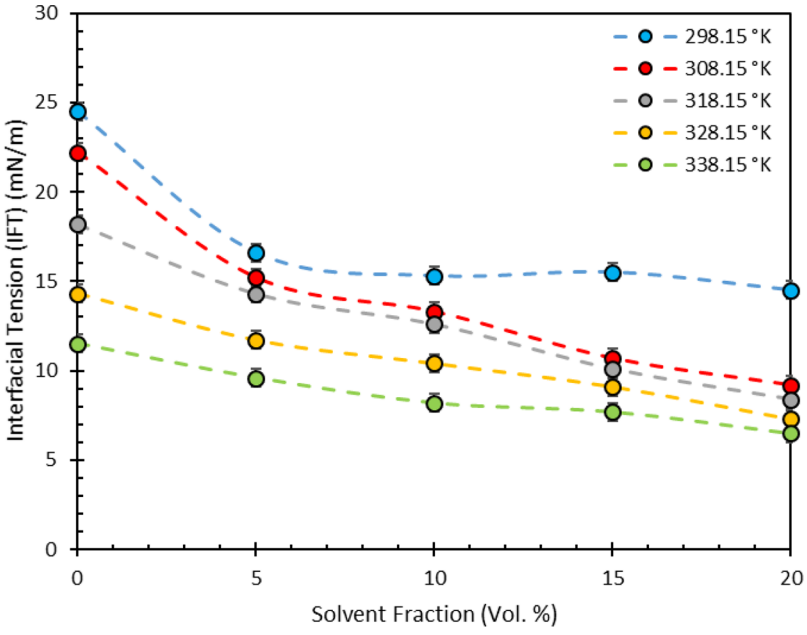

Figure 20. IFT measurements for AVBP solution versus ethanol solvent at different concentrations and temperatures at P = 14.7 psi; concentration= 1 g/100 mL.

for the polymer solution containing different volume percentages of ethanol at different temperatures. It can be observed that increasing the temperature has a positive effect on reducing the CA values and increasing the hydrophilicity of the rock. Similarly, increasing the volume percentage of ethanol decreased the CA values. Moreover, the increase in the temperature also acts as a catalyst, accelerating CA reduction. In addition, this experiment proved that AVBP works efficiently at reservoir temperatures and can be utilized for practical field operations. The free energy between the oil phase and the solution is decreased at high temperatures. This phenomenon increases the mobility of the crude oil and the key at the interface, resulting in lower intermolecular forces. Thus, CA values are reduced at higher temperatures, resulting in a more water-wet state at higher temperatures.[77,78,80,81]

3.2.5.3. CA Measurements of AVBP–Ethanol–NC Solutions. Figure 24 exhibits the CA measurements for the AVBP–ethanol solution at different concentrations of the NC. Due to their dimensions, nanomaterials can be effective in reservoirs with small pore sizes. One of the main mechanisms of nanomaterials is the wettability alteration of rock surfaces. Therefore, the primary purpose of these nanomaterials is to enter the tiny rock pores and alter the rock's wettability. Figure 24 shows that the CA values decreased with increasing concentration of NC. In this part of the experiment, the CA reduction is due to the wettability alteration of the rock toward water wetness. Initially, increasing the concentration of NC to

https://doi.org/10.1021/acsomega.3c05921
ACS Omega 2023, 8, 43930−43954

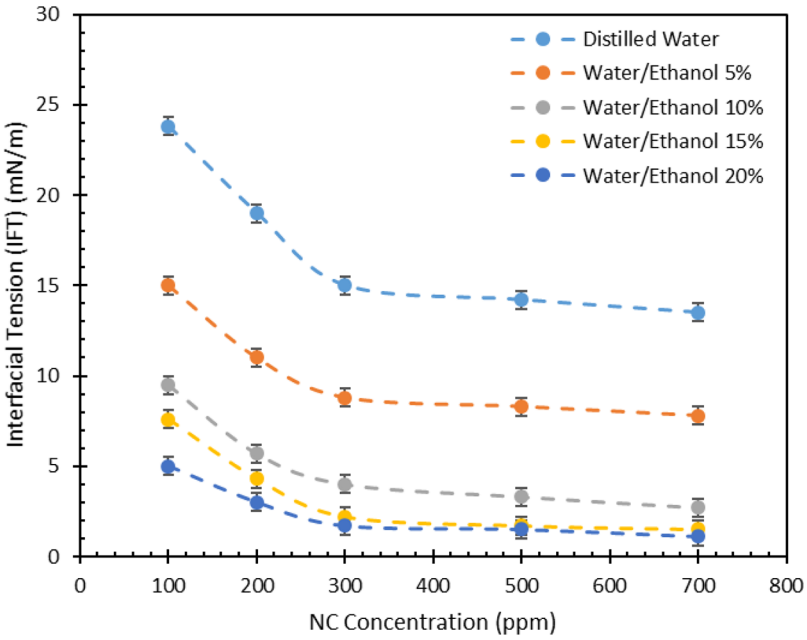

Figure 21. IFT measurements for AVBP (1 g/100 mL) versus different concentrations of NC in various solvent fractions (ethanol).

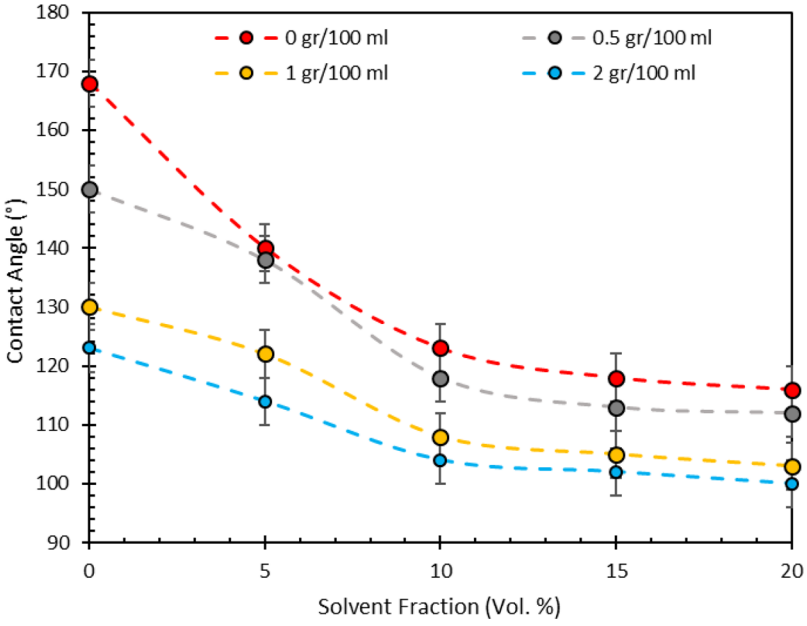

Figure 22. Measurements for various AVBP solutions and sandstone rock samples versus different concentrations of ethanol solvent at P = 14.7 psi and T = 298.15 °K.

300 ppm reduced the CA values with a considerable slope. Beyond the concentration of 300 ppm, the CA reduction slowed and reached almost a plateau. Increasing the concentration of the NC beyond this level results in the disjoint pressure mechanism and reduces the CA. Hence, it can be observed that there is a threshold (in this case, 300 ppm) beyond which increasing the concentration of NC is ineffective. Due to its dual structure (a hydrophilic head and a hydrophobic head), ethanol can act as a surfactant and alter the rock surface toward a water-wet state by forming semimicelles. Furthermore, adding the ethanol solvent up to 10% by volume reduced the CA efficiently. Further addition of ethanol solvent to the solution did not markedly reduce the CA values.[4,77,82]

3.3. Dynamic Tests. In this section, the obtained optimum solutions from batch experiments were used in the core flooding experiments to further study the solutions' dynamic behavior in conditions more representative of the reservoir. Table 9 summarizes the different solutions selected for the flooding tests and their IFT and CA values. Moreover, the performance of each solution is compared to a benchmark (DWI or AVBP). The pressure drop and RF are plotted for each test, as shown in Figure 25. Water flooding was conducted as a benchmark for the flooding experiments (Figure 25a). The recovery of water flooding (after injecting four PVs) was roughly 50%. The recovery of water flooding did not change noticeably beyond two PVs of water injection. A

https://doi.org/10.1021/acsomega.3c05921
ACS Omega 2023, 8, 43930−43954

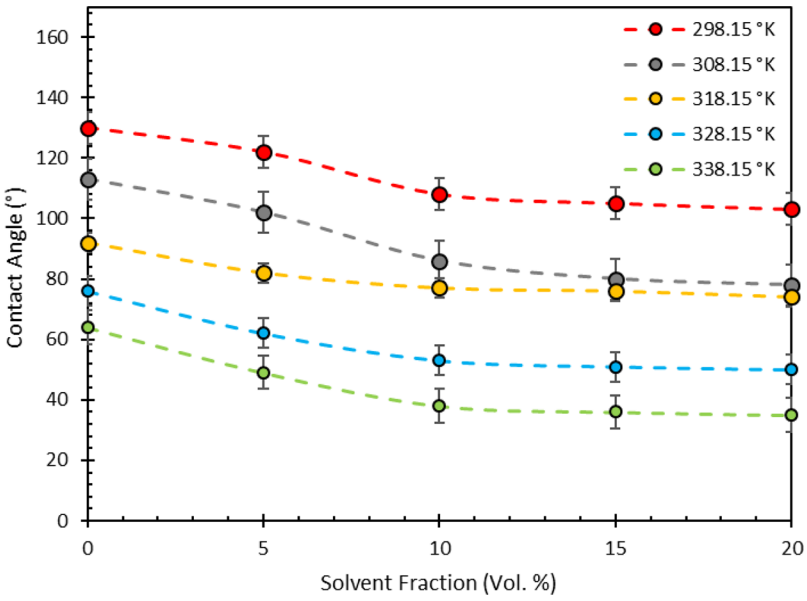

Figure 23. Measurements for AVBP solution and sandstone rock sample versus various concentrations of ethanol solvent at different temperatures @ P = 14.7 psi; concentration= 1 gr/100 mL

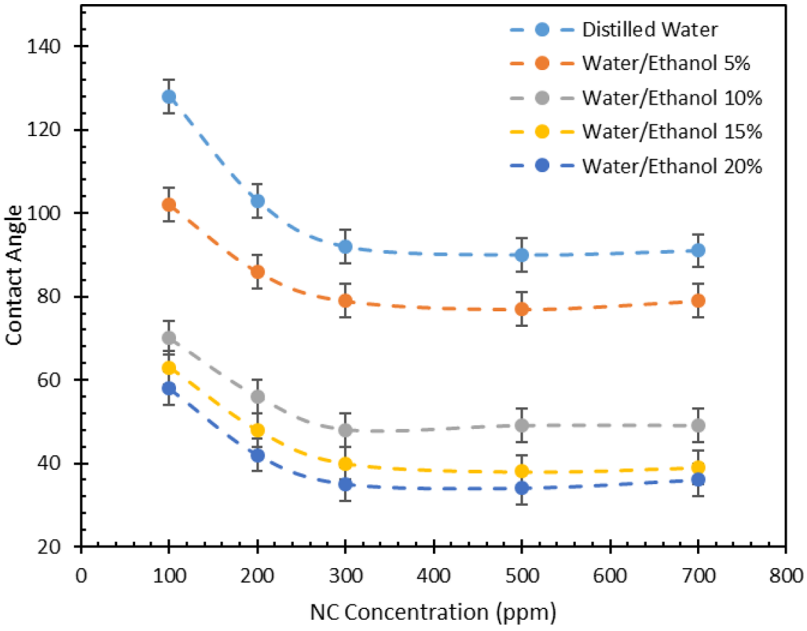

Figure 24. Measurements for AVBP (1 g/100 mL) versus different concentrations of NC in various concentrations of ethanol solvent.

Table 9. Optimization and the Value of Solution Used in the Core Flooding Test

	IFT			contact angle		
solution	value	optimization	compare with	value	optimization	compare with
AVBP (1 g/100 mL)/DW	24.5 mN/m	23.67%	DW[a]	130°	22.62%	DW[b]
AVBP (1 g/100 mL)/ethanol 10%	15.3 mN/m	52.33%	DW	108°	55.56%	DW
	15.3 mN/m	37.55%	AVBP	108°	16.92%	AVBP
AVBP (1 g/100 mL)/ethanol 10%/NC (300 ppm)	4 mN/m	87.53%	DW	48°	71.42%	DW
	4 mN/m	83.76%	AVBP	48°	63.03%	AVBP

[a]IFT_DW= 32.1 mN/m. [b]Contact angle = 168°.

steep pressure drop happened around the injection of 1 PV, indicating an early water breakthrough.

The second flooding test used the polymer solution (Figure 25b). In the following two tests, ethanol solvent and NC material were added to the system to further enhance the polymer solution's performance (Figure 25c,d). While the polymer improves the sweep efficiency of an injected CEOR agent, the addition of ethanol and NC decreases the IFT and

https://doi.org/10.1021/acsomega.3c05921
ACS Omega 2023, 8, 43930−43954

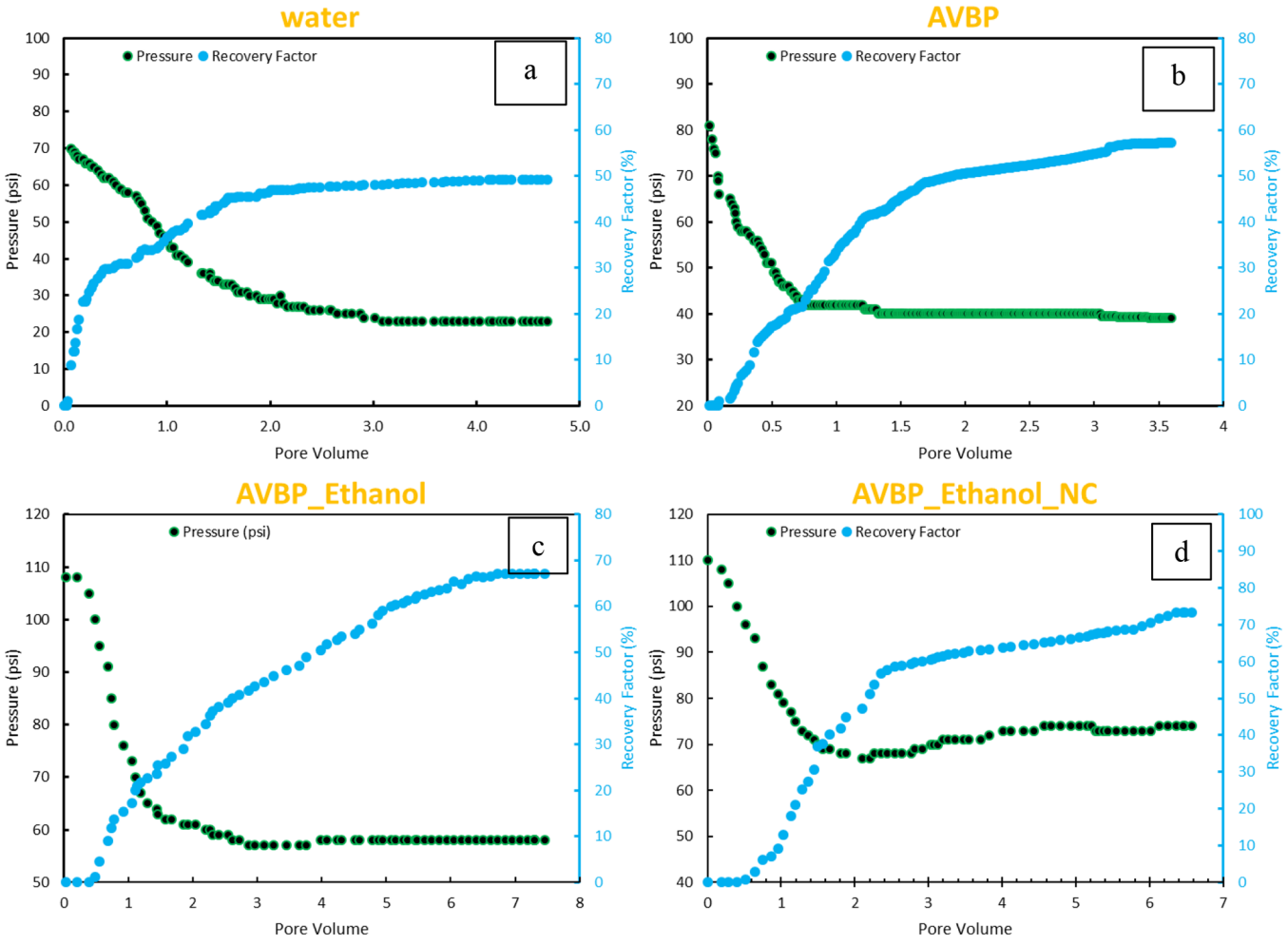

Figure 25. Recovery factor and pressure drop curves for different core flooding scenarios: water flooding (a), AVBP (b), AVBP+ethanol (c), and AVBP_Ethanol_NC (d).

CA values, respectively. As shown in Figure 25b, for tests in which the polymer solution was injected, the injection pressure diagram showed a higher injection pressure than the reference case, which can be attributed to the viscosity of the polymer solution. The recovery of polymer flooding is substantially higher than that of water injection (10% higher), and the breakthrough happened later in the injection process. This can be attributed to the more uniform displacement resulting from the enhanced sweep efficiency of polymers compared to that of water flooding. Moreover, the recovery plateau was observed much later than that of the water flooding (around 3 PVs). The ultimate RFs of AVBP−ethanol and AVBP−ethanol−NC were substantially higher than those for water flooding and polymer injection at 69 and 73%, respectively. The breakthrough in both cases occurred beyond the injection of two PVs of fluid. This indicated that using an AVBP−ethanol−NC solution can result in high oil recovery (23% higher than water flooding) and hence can be considered to be the optimum CEOR candidate for the reservoir of interest.

3.3.1. Relative Permeability Analysis. The relative permeability curves were plotted by using the Corey correlation model. Figure 26 illustrates the relative permeability diagrams for the four tests. As can be seen, with the addition of the polymer solution to the system, the mobility of oil and, consequently, the oil recovery have increased significantly. The method proposed by Mirzaei-Paiaman et al.[56,79] has been used to analyze the relative permeability diagrams quantitatively. As shown in Figure 27, the suggested process converts the relative permeability curves into numerical indices representing wettability. Table 10 summarizes the constant values and required parameters for this method. The closer the index is to −1, the more oil-wet the rock surface is. On the other hand, the closer the index is to + 1, the rock is considered to be more water-wet. Figure 27 shows that AVBP−ethanol−NC further shifted the wettability toward a more water-wetness state than the rest of the CEOR scenarios used in this study. Changing the wettability of rock toward water-wetness could be attributed to the combined effect of NC and ethanol. Consequently, the system's final recovery for this test was higher than others.

Figure 28 depicts fractional flow (fw) curves vs water saturation. As illustrated, adding polymer to the system has shifted these curves to the right. This indicates that adding the polymer solution resulted in a more piston-like front movement in the reservoir. Moreover, the front saturation (Swf injection) is recorded for each injected fluid. The Swf values were 0.48, 0.62, 0.64, and 0.66 for water flooding, polymer flooding, AVBP−ethanol, and AVBP−ethanol−NC, respectively. When the solution of AVBP−ethanol−NC is injected, the Swf at the front has increased considerably from 0.48 to 0.62 in contrast to the water flooding (benchmark). This indicates a more efficient flooding process. Furthermore,

https://doi.org/10.1021/acsomega.3c05921
ACS Omega 2023, 8, 43930−43954

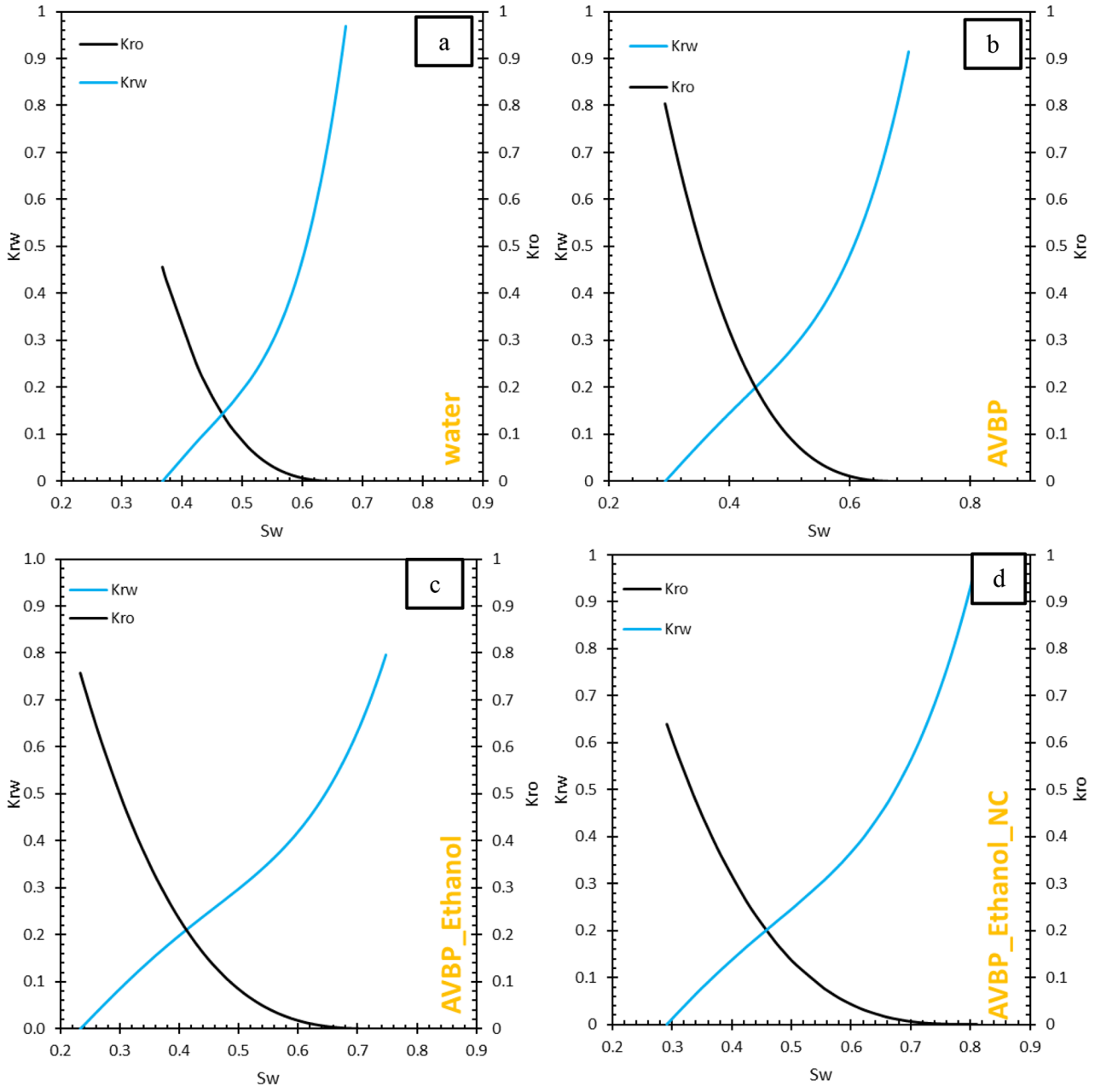

Figure 26. Relative permeability curves for (a) water, (b) AVBP, (c) AVBP+ethanol, and (d) AVBP+ethanol+NC core flooding scenarios using the Corey correlation model.

the oil recovery at the breakthrough time for each curve was calculated, as shown in Table 11. It can be observed that both ultimate recovery and recovery at breakthrough are highest when AVBP−ethanol−NC is used as a CEOR agent.

3.3.2. Capillary Number and Mobility Ratio. Table 12 summarizes the capillary numbers and mobility ratios of different CEOR fluids used in this study. The mobility ratio of DIW is 71, indicating that the water flooding results in poor recovery due to the low sweep efficiency and early fingering. That could be one of the main reasons for the 27.2% recovery of DIW. As expected, adding AVBP, AVBP−ethanol, and AVBP−ethanol−NC markedly enhanced the mobility ratios to 3.81, 2.29, and 1.69, respectively. Ethanol and NC have resulted in a reduction in mobility ratio, although not substantially.

On the other hand, the main effect is more apparent in microscopic displacement efficiency, as indicated by the capillary numbers in Table 12. Higher capillary numbers indicate that viscous forces prevail over the capillary forces. This results in mobilization of the trapped oil and an increase in the recovery. It is widely accepted that in EOR operations, when NC numbers exceed 10^{-4}, the trapped (residual oil) is mobilized. As the table shows, adding polymer improves the capillary number by two orders of magnitude to 2×10^{-4}. However, adding ethanol pushes the values over the effectiveness threshold (values higher than 10^{-4}). As NC is added, N_{Ca} is further improved. The increased capillary numbers indicate that microscopic sweep efficiency is high. The RFs can be explained by improving mobility ratio and capillary numbers, which ultimately resulted in the highest recoveries of 57.64, 55.07, and 48.99% for AVBP−ethanol−

https://doi.org/10.1021/acsomega.3c05921
ACS Omega 2023, 8, 43930−43954

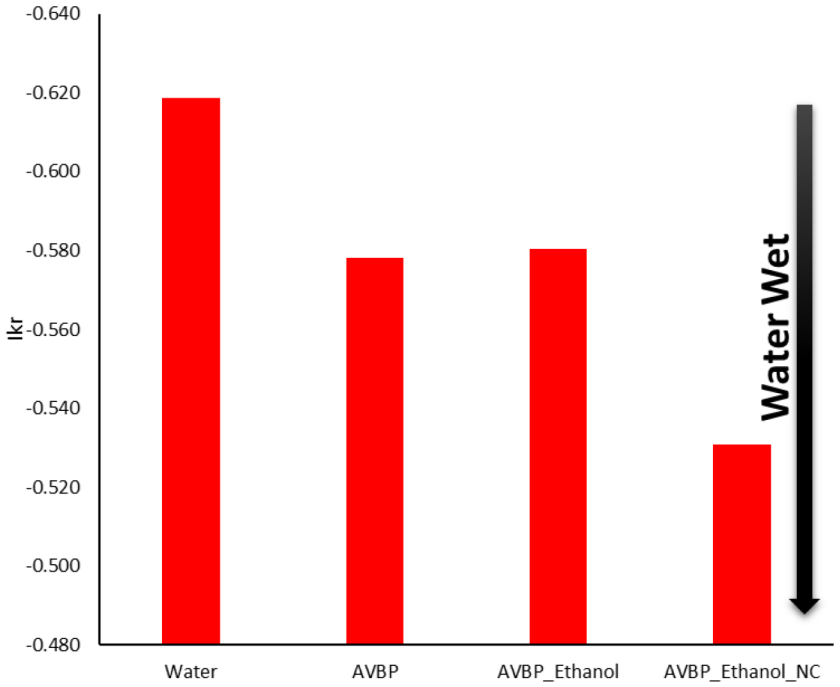

Figure 27. Lak wettability index for analyzing relative permeability curves.

Table 10. Parameters and Constant Values for the Lak Wettability Index Method for Analyzing the Relative Permeability Curves

solution sample	K_{rw}@ROS	IWS (%)	ROS (%)	CS (%)	RCS (%)	S_{or}	I_{kr1}	I_{kr2}	I_{kr}
water	0.914	0.368	0.679	0.460	0.524	0.3208	−0.414	−0.205	−0.619
AVBP	0.914	0.294	0.698	0.430	0.496	0.302	−0.414	−0.164	−0.578
AVBP−ethanol	0.951	0.233	0.738	0.420	0.486	0.2619	−0.451	−0.130	−0.580
AVBP−ethanol−NC	0.970	0.292	0.811	0.420	0.552	0.1887	−0.470	−0.061	−0.531

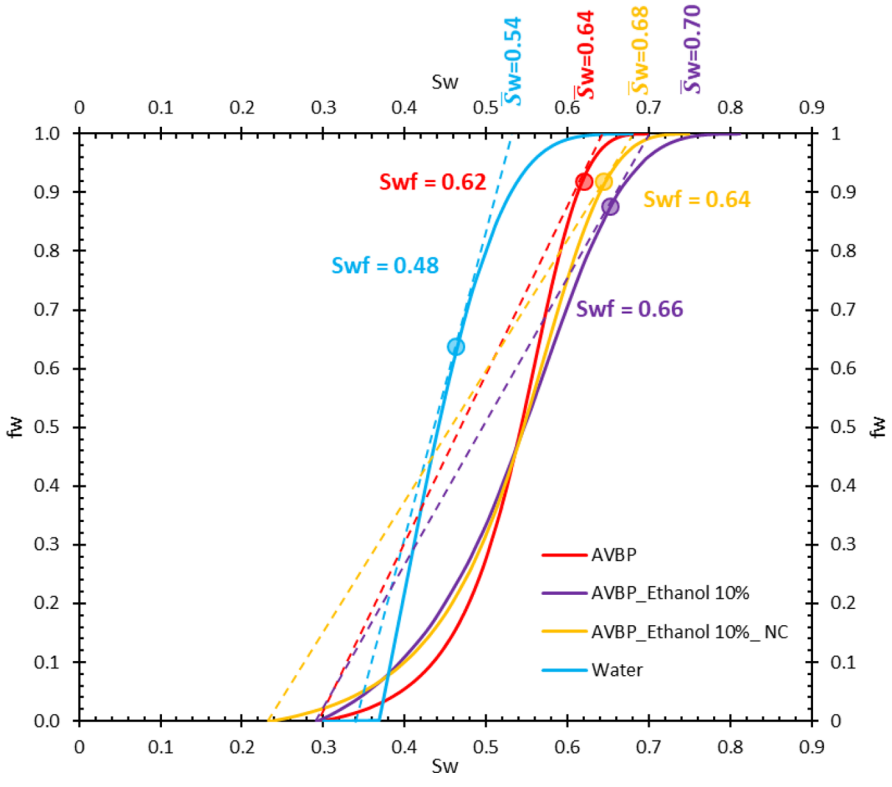

Figure 28. Fractional flow curves for different core flooding scenarios.

https://doi.org/10.1021/acsomega.3c05921
ACS Omega 2023, 8, 43930−43954

Table 11. Recovery Factor Measurements for Each Test

solution sample	S_{wi}	final recovery	S_w	recovery factor at breakthrough
water	0.3681	49.22%	0.54	27.20%
AVBP	0.2943	57.21%	0.64	48.99%
AVBP−ethanol	0.2878	67.15%	0.68	55.07%
AVBP−ethanol−NC	0.2918	73.35%	0.70	57.64%

Table 12. Capillary Number and Mobility Ratio of the Different CEOR Agents

CEOR agent	N_{Ca}	M
DWI	8.4×10^{-6}	71.28
AVBP	2.0×10^{-4}	3.81
AVBP−ethanol	1.0×10^{-3}	2.29
AVBP−ethanol−NC	2.8×10^{-3}	1.62

NC, AVBP−ethanol, and AVBP, respectively. The difference between recoveries of AVBP−ethanol−NC and AVBP−ethanol is 2%. However, for practical applications, the economics of the operation will be the crucial factor in deciding the proper CEOR agent(s). Hence, creating a situation with a low mobility ratio and low capillary number values facilitates oil production during chemical flooding. Therefore, the application of AVBP−ethanol−NC as the flooding agent assists the incremental oil recovery in this study.[1,4,54]

4. CONCLUSIONS

In this study, several batches and flooding experiments were conducted to examine the application of a novel, environmentally friendly biobased polymer (AVBP) for CEOR purposes. A comprehensive polymer characterization using various techniques was performed in the first set of experiments. Subsequently, the polymer rheology, adsorption, and stability were investigated in the presence of different brines. In the next part, the properties of the polymeric solution at different volume percentages of ethanol were evaluated. Finally, the synergism of the polymer with a new NC was studied. Flooding tests were conducted on sandstone core plugs in the next series of experiments. Various parameters such as the RF, relative permeability, wettability after injection, and fraction flow analysis were studied for each CEOR scenario (using water flooding as a benchmark). These results of batch experiments are summarized as follows:

- FTIR and ^{1}H NMR analyses were applied for structural and functional group determination. The results proved the presence of polysaccharide structures in the AVBP. The TGA test demonstrated that 17.78% of the initial weight of the polymer was lost at the reservoir temperature. Therefore, the polymer is thermally stable and can be used suitably as a CEOR agent.
- The compatibility tests revealed no precipitation between the polymer solution and brine containing salinities up to 80,000 (at 25 °C).
- Rheological evaluation of this polymer solution showed that it has Newtonian behavior and could be well-explained by applying the Herschel−Bulkley model.
- UV-spectroscopy apparatus was utilized for polymer adsorption determination. It was shown that the λ_{max} was 330 nm, and the final adsorption at concentrations of 0.5, 1, and 2 g/100 mL was 2.2, 2.4, and 2.8 a.u, respectively.
- The IFT and CA of the polymer solution were improved by adding ethanol to the system. For the AVBP−ethanol system, a volume percentage of 10% was determined as the optimal concentration and the IFT and CA values were enhanced by 52.33 and 55.56%, respectively. Further addition of NC with an optimum concentration of 300 ppm was added to the polymer and ethanol systems and improved the IFT and CA values by 87.53 and 71.42%, respectively.
- The AVBP−ethanol−NC solution's flooding test resulted in the highest oil recovery of 73.35%. This was a 24.13% improvement from that of water flooding.
- Two-phase relative permeability analysis proved the wettability alternation of the AVBP−ethanol−NC system, and the resulting improvement of relative permeability to oil contributed to increasing RF.
- Fractional flow analysis showed that through the synergetic effects of the AVBP−ethanol−NC solution, a more uniform displacement and higher recoveries are attainable.

The result of the experiments indicated that the AVBP−ethanol−NC system improves oil recovery using a combination of different mechanisms, such as mobilization of oil due to the IFT reduction achieved through using ethanol and NC, improvement of sweep efficiency as a result of adding AVBP to the solution, and finally changing the wettability of sandstone rock samples toward more water-wet conditions through the synthetic effect of AVBP−ethanol−NC. Therefore, AVBP−ethanol−NC could be an effective CEOR method for the reservoir of interest.

AUTHOR INFORMATION

Corresponding Author

Erfan Mohammadian − *Key Laboratory of Continental Shale Hydrocarbon Accumulation and Efficient Development, Ministry of Education and Joint International Research Laboratory of Unconventional Energy Resources, Northeast Petroleum University, Daqing 163318, China;* orcid.org/0000-0002-7362-5031; Email: Erfan.723@gmail.com

Authors

Abbas Khaksar Manshad − *Department of Petroleum Engineering, Abadan Faculty of Petroleum, Petroleum University of Technology (PUT), Abadan 49658-15879, Iran*

Alireza Kabipour − *Department of Petroleum Engineering, Abadan Faculty of Petroleum, Petroleum University of Technology (PUT), Abadan 49658-15879, Iran*

Lei Yan − *Department of Chemistry, Tsinghua University, Beijing 100084, China*

Jagar A. Ali − *Department of Petroleum Engineering, Faculty of Engineering and Scientific Research Centre, Soran University, Soran, Kurdistan Region 44008, Iraq*

Stefan Iglauer − *Petroleum Engineering Discipline, School of Engineering and Centre for Sustainable Energy and Resources, Edith Cowan University, Joondalup, WA 6027, Australia;* orcid.org/0000-0002-8080-1590

Alireza Keshavarz − *Petroleum Engineering Discipline, School of Engineering and Centre for Sustainable Energy and Resources, Edith Cowan University, Joondalup, WA 6027, Australia;* orcid.org/0000-0002-8091-961X

https://doi.org/10.1021/acsomega.3c05921
ACS Omega 2023, 8, 43930−43954

Milad Norouzpour − *Department of Petroleum Engineering, Marvdasht Branch, Islamic Azad University, Marvdasht 73711-13119, Iran*
Amin Azdarpour − *Department of Petroleum Engineering, Marvdasht Branch, Islamic Azad University, Marvdasht 73711-13119, Iran;* orcid.org/0000-0001-7826-2025
S. Mohammad Sajadi − *Department of Nutrition, Cihan University, Erbil, KRG 10320, Iraq*
Siyamak Moradi − *Department of Petroleum Engineering, Abadan Faculty of Petroleum, Petroleum University of Technology (PUT), Abadan 49658-15879, Iran*

Complete contact information is available at: https://pubs.acs.org/10.1021/acsomega.3c05921

Notes

The authors declare no competing financial interest.

■ ACKNOWLEDGMENTS

The authors wish to thank the Key R&D Program of Heilongjiang Province (GA23A906) and Northeast Petroleum University for providing the National (Cultivation) Fund (2023GPL-05) that made this work possible.

■ NOMENCLATURE

CEOR	chemical enhanced oil recovery
EOR	enhanced oil recovery
AVBP	Aloe Vera biopolymer
XRD	X-ray diffraction
NC	nanocomposite
IFT	interfacial tension
DIW	deionized water
FTIR	Fourier-transform infrared spectroscopy
TGA	thermogravimetric analysis
NMR	nuclear magnetic resonance
SEM	scanning electron microscopy
PAM	polyacrylamide polymer
LSW	low-salinity water
FW	formation water
SW	water saturation
fw	fractional flow
K_r	relative permeability
RF	recovery factor
Swc	water saturation
TDS	total dissolved salinity
UV-S	ultraviolet−visible spectroscopy

■ REFERENCES

(1) Azdarpour, A.; Mohammadian, E.; Norouzpour, M.; Liu, B. The Effects of a Novel Bio-Based Surfactant Derived from the Acacia Concinna Plant on Chemical Enhanced Oil Recovery in the Presence of Various Salts and a Synthesized HSPAM Polymer. *J. Mol. Liq.* **2023**, *386*, No. 122474.
(2) Norouzpour, M.; Nabipour, M.; Azdarpour, A.; Santos, R. M. Isolating the Effect of asphaltene Content on Enhanced Oil Recovery during Low Salinity Water Flooding of Carbonate Reservoirs. *Energy Sources, Part A* **2020**, 1−14.
(3) Sami, B.; Azdarpour, A.; Honarvar, B.; Nabipour, M.; Keshavarz, A. Application of a Novel Natural Surfactant Extracted from Avena Sativa for Enhanced Oil Recovery during Low Salinity Water Flooding: Synergism of Natural Surfactant with Different Salts. *J. Mol. Liq.* **2022**, *362*, No. 119693.
(4) Azdarpour, A.; Norouzpour, M.; Nabipour, M.; Santos, R. M.; Mohammadian, E.; Ostadhassan, M. Efficiency of the Green Surfactant Derived from *Avena Sativa* Plant in the Presence of Different Salts for EOR Purposes. *J. GeoEnergy* **2023**, *2023*, No. 9998466.
(5) Qazvini, S.; Golkari, A.; Azdarpour, A.; Santos, R. M.; Safavi, M. S.; Norouzpour, M. Experimental and Modelling Approach to Investigate the Mechanisms of Formation Damage Due to Calcium Carbonate Precipitation in Carbonate Reservoirs. *J Pet Sci Eng* **2021**, *205*, No. 108801.
(6) Honarvar, B.; Azdarpour, A.; Karimi, M.; Rahimi, A.; Afkhami Karaei, M.; Hamidi, H.; Ing, J.; Mohammadian, E. Experimental Investigation of Interfacial Tension Measurement and Oil Recovery by Carbonated Water Injection: A Case Study Using Core Samples from an Iranian Carbonate Oil Reservoir. *Energy & Fuels* **2017**, *31*, 2740−2748.
(7) Norouzpour, M.; Azdarpour, A.; Nabipour, M.; Santos, R. M.; Khaksar Manshad, A.; Iglauer, S.; Akhondzadeh, H.; Keshavarz, A. Red Beet Plant as a Novel Source of Natural Surfactant Combined with 'Smart Water' for EOR Purposes in Carbonate Reservoirs. *J. Mol. Liq.* **2023**, *370*, No. 121051.
(8) Ahsaei, Z.; Nabipour, M.; Azdarpour, A.; Santos, R. M.; Mohammadian, E.; Babakhani, P.; Hamidi, H.; Karaei, M. A.; Esfandiarian, A. Application of Commercial Zwitterionic Surfactants and Ionic Liquids to Reduce Interfacial Tension and Alter Wettability in a Carbonate Reservoir. *Energy Sources, Part A: Recovery, Utilization, and Environmental Effects* **2022**, *44*, 2811−2822.
(9) Zeng, Y.; Kamarul Bahrim, R. Z.; Groot, J.A.W.M.; Vincent-Bonnieu, S.; Groenenboom, J.; Mohd Shafian, S. R.; Abdul Manap, A. A.; Tewari, R. D.; Mohammadian, E.; Azdarpour, A.; et al. Probing Methane Foam Transport in Heterogeneous Porous Media: An Experimental and Numerical Case Study of Permeability-Dependent Rheology and Fluid Diversion at Field Scale. *SPE Journal* **2020**, *25*, 1697−1710.
(10) Ahmadi, Y. Improving Fluid Flow Through Low Permeability Reservoir in the Presence of Nanoparticles: An Experimental Core Fooding WAG Tests. *Iran. J. Oil Gas Sci. Technol.* **2021**, *12*, doi: DOI: 10.22050/ijogst.2021.287297.1595.
(11) Ahmadi, Y.; Javadi, F.; Kikhavandi, T. Effect of Different Salinity on Low Permeability Carbonate Reservoir Recovery Using a New Green Polymeric Nanocomposites. *Energy Sources, Part A: Recovery, Utilization, and Environmental Effects* **2023**, *45*, 1091−1103.
(12) Jafarbeigi, E.; Ahmadi, Y.; Mansouri, M.; Ayatollahi, S. Experimental Core Flooding Investigation of New ZnO−γAl2O3 Nanocomposites for Enhanced Oil Recovery in Carbonate Reservoirs. *ACS Omega* **2022**, *7*, 39107−39121.
(13) Mansouri, M.; Jafarbeigi, E.; Ahmadi, Y.; Hosseini, S. H. Experimental Investigation of the Effect of Smart Water and a Novel Synthetic Nanocomposite on Wettability Alteration, Interfacial Tension Reduction, and EOR. *J Pet Explor Prod Technol* **2023**, *13*, 2251−2266.
(14) Sveistrup, M.; van Mastrigt, F.; Norrman, J.; Picchioni, F.; Paso, K. Viability of Biopolymers for Enhanced Oil Recovery. *J Dispers Sci Technol* **2016**, *37*, 1160−1169.
(15) Yu, L.; Dean, K.; Li, L. Polymer Blends and Composites from Renewable Resources. *Prog. Polym. Sci.* **2006**, *31*, 576−602.
(16) Mansoori, S.; Davarnejad, R.; Matsuura, T.; Ismail, A. Membranes Based on Non-Synthetic (Natural) Polymers for Wastewater Treatment. *Polym Test* **2020**, *84*, No. 106381.
(17) Nayak, A. K.; Hasnain, M. S.; Behera, A.; Dhara, A. K.; Pal, D. Chapter 15 - Biological Macromolecules in Drug Delivery. In *Biological Macromolecules*; Nayak, A. K.; Dhara, A. K.; Pal, D., Eds.; Academic Press, 2022; pp. 339−379 ISBN 978−0-323−85759−8, DOI: 10.1016/B978-0-323-85759-8.00015-4.
(18) Ling, F. W. M.; Abdulbari, H. A.; Kadhum, W. A.; Heng, J. T. Investigating the Flow Behavior of Dilute Aloe Vera Biopolymer Solutions in Microchannel. *Chem. Eng. Commun.* **2021**, *208*, 753−763.
(19) Citations-20230924T055133z.
(20) Goudarzi, A.; Zhang, H.; Varavei, A.; Taksaudom, P.; Hu, Y.; Delshad, M.; Bai, B.; Sepehrnoori, K. A Laboratory and Simulation

Study of Preformed Particle Gels for Water Conformance Control. *Fuel* **2015**, *140*, 502−513.
(21) Hassan, A. M.; Ayoub, M.; Eissa, M.; Musa, T.; Bruining, H.; Farajzadeh, R. Exergy Return on Exergy Investment Analysis of Natural-Polymer (Guar-Arabic Gum) Enhanced Oil Recovery Process. *Energy* **2019**, *181*, 162−172.
(22) Hamdi, S. S.; Al-Kayiem, H. H.; Muhsan, A. S. Natural Polymer Non-Covalently Grafted Graphene Nanoplatelets for Improved Oil Recovery Process: A Micromodel Evaluation. *J. Mol. Liq.* **2020**, *310*, No. 113076.
(23) Nowrouzi, I.; Mohammadi, A. H.; Khaksar Manshad, A. Characterization and Likelihood Application of Extracted Mucilage from Hollyhocks Plant as a Natural Polymer in Enhanced Oil Recovery Process by Alkali-Surfactant-Polymer (ASP) Slug Injection into Sandstone Oil Reservoirs. *J. Mol. Liq.* **2020**, *320*, No. 114445.
(24) Ahmadi, Y.; Ayari, M. A.; Olfati, M.; Hosseini, S. H.; Khandakar, A.; Vaferi, B.; Olazar, M. Application of Green Polymeric Nanocomposites for Enhanced Oil Recovery by Spontaneous imbibition from Carbonate Reservoirs. *Polymers* **2023**, *15*, 3064.
(25) Sharma, T.; Sangwai, J. S. Silica Nanofluids in Polyacrylamide with and without Surfactant: Viscosity, Surface Tension, and Interfacial Tension with Liquid Paraffin. *J Pet Sci Eng* **2017**, *152*, 575−585.
(26) Saha, R.; Uppaluri, R. V. S.; Tiwari, P. Silica Nanoparticle Assisted Polymer Flooding of Heavy Crude Oil: Emulsification, Rheology, and Wettability Alteration Characteristics. *Ind. Eng. Chem. Res.* **2018**, *57*, 6364.
(27) Esfandyari Bayat, A.; Junin, R.; Samsuri, A.; Piroozian, A.; Hokmabadi, M. Impact of Metal Oxide Nanoparticles on Enhanced Oil Recovery from Limestone Media at Several Temperatures. *Energy & Fuels* **2014**, *28*, 6255−6266.
(28) Li, Y.; Dai, C.; Zhou, H.; Wang, X.; Lv, W.; Zhao, M. Investigation of Spontaneous imbibition by Using a Surfactant-Free Active Silica Water-Based Nanofluid for Enhanced Oil Recovery. *Energy Fuels* **2018**, *32*, 287.
(29) Ehtesabi, H.; Ahadian, M. M.; Taghikhani, V.; Ghazanfari, M. H. Ghazanfari, mohammad hossein Enhanced Heavy Oil Recovery in Sandstone Cores Using TiO2 Nanofluids. *Energy Fuels* **2013**, *28*, 423−430.
(30) Cheraghian, G. Effect of Nano Titanium Dioxide on Heavy Oil Recovery during Polymer Flooding. *Pet Sci Technol* **2016**, *34*, 633−641.
(31) Cheraghian, G. Effects of Titanium Dioxide Nanoparticles on the Efficiency of Surfactant Flooding of Heavy Oil in a Glass Micromodel. *Pet Sci Technol* **2016**, *34*, 260−267.
(32) Kazemzadeh, Y.; Sharifi, M.; Riazi, M.; Rezvani, H.; Tabaei, M. Potential Effects of Metal Oxide/SiO2 Nanocomposites in EOR Processes at Different Pressures. *Colloids Surf A Physicochem Eng Asp* **2018**, *559*, 372−384.
(33) Nowrouzi, I.; Mohammadi, A. H.; Manshad, A. K. Primary Evaluation of a Synthesized Surfactant from Waste Chicken Fat as a Renewable Source for Chemical Slug Injection into Carbonate Oil Reservoirs. *J. Mol. Liq.* **2020**, *306*, No. 112843.
(34) Mehrabianfar, P.; Malmir, P.; Soulgani, B. S.; Hashemi, A. Study on the Optimization of the Performance of Preformed Particle Gel (PPG) on the Isolation of High Permeable Zone. *J Pet Sci Eng* **2020**, *195*, No. 107530.
(35) Esfandiarian, A.; Maghsoudian, A.; Shirazi, M.; Tamsilian, Y.; Kord, S.; Sheng, J. Mechanistic Investigation of the Synergy of a Wide Range of salinities and Ionic Liquids for Enhanced Oil Recovery: Fluid−Fluid Interactions. *Energy & Fuels* **2021**, *35*, 3011−3031.
(36) Nazarahari, M. J.; Manshad, A. K.; Ali, M.; Ali, J. A.; Shafiei, A.; Sajadi, S. M.; Moradi, S.; Iglauer, S.; Keshavarz, A. Impact of a Novel Biosynthesized Nanocomposite (SiO2@Montmorilant@Xanthan) on Wettability Shift and Interfacial Tension: Applications for Enhanced Oil Recovery. *Fuel* **2021**, *298*, No. 120773.
(37) Hsissou, R.; Seghiri, R.; Benzekri, Z.; Hilali, M.; Rafik, M.; Elharfi, A. Polymer Composite Materials: A Comprehensive Review. *Compos Struct* **2021**, *262*, No. 113640.
(38) Ravindran, L.; Sreekala, M. S.; Goda, K.; Thomas, S. Chapter 1 - The State of the Art of Biopolymers-New Challenges, Opportunities, and Future Prospects. In *Handbook of Natural Polymers, Volume 1*; Sreekala, M. S.; Ravindran, L.; Goda, K.; Thomas, S., Eds.; Elsevier, 2023; pp. 1−18 ISBN 978−0-323−99853−6, DOI: 10.1016/B978-0-323-99853-6.00023-1.
(39) Thakur, M.; Sharma, A.; Chandel, M.; Pathania, D. Chapter 9 - Modern Applications and Current Status of Green Nanotechnology in Environmental Industry. In *Green Functionalized Nanomaterials for Environmental Applications*; Shanker, U.; Hussain, C. M.; Rani, M., Eds.; Elsevier, 2022; pp. 259−281 ISBN 978−0-12−823137−1, DOI: 10.1016/B978-0-12-823137-1.00010-5.
(40) Ali, J.; Hamadamin, A.; Ahmed, S.; Mahmood, B.; Sajadi, S. M.; Manshad, A. Synergistic Effect of Nanoinhibitive Drilling Fluid on the Shale Swelling Performance at High Temperature and High Pressure. *Energy Fuels* **2022**, *36*, 1996.
(41) Bagalkot, N.; Hamouda, A. A.; Isdahl, O. M. Dynamic Interfacial Tension Measurement Method Using Axisymmetric Drop Shape Analysis. *MethodsX* **2018**, *5*, 676−683.
(42) Ghorbani, M.; Mohammadi, A. H. Effects of Temperature, Pressure and Fluid Composition on Hydrocarbon Gas - Oil Interfacial Tension (IFT): An Experimental Study Using ADSA Image Analysis of Pendant Drop Test Method. *J. Mol. Liq.* **2017**, *227*, 318−323.
(43) Meiron, T.; Marmur, A.; Saguy, I. S. Measurement on Rough Surfaces. *J. Colloid Interface Sci.* **2004**, *274*, 637−644.
(44) Kumar, K.; Chauhan, S. Surface Tension and UV−Visible Investigations of Aggregation and Adsorption Behavior of NaC and NaDC in Water−Amino Acid Mixtures. *Fluid Phase Equilib.* **2015**, *394*, 165−174.
(45) Vedhanayagam, M.; Andra, S.; Muthalagu, M.; Sreeram, K. J. Influence of Functionalized Gold Nanorods on the Structure of Cytochrome − C: An Effective Bio-Nanoconjugate for Biomedical Applications. *Inorg. Chem. Commun.* **2022**, *146*, No. 110182.
(46) Ponder, J.F.Jr.; Österholm, A. M.; Reynolds, J. R. Conjugated Polyelectrolytes as Water Processable Precursors to Aqueous Compatible Redox Active Polymers for Diverse Applications: Electrochromism, Charge Storage, and Biocompatible Organic Electronics. *Chem. Mater.* **2017**, *29*, 4385−4392.
(47) Liu, M.; Blankenship, J. R.; Levi, A. E.; Fu, Q.; Hudson, Z. M.; Bates, C. M. Miktoarm Star Polymers: Synthesis and Applications. *Chem. Mater.* **2022**, *34*, 6188−6209.
(48) Kim, D.; Kim, F. S. Materials Chemistry, Device Engineering, and Promising Applications of Polymer Transistors. *Chem. Mater.* **2021**, *33*, 7572−7594.
(49) Advincula, A. A.; Jones, A. L.; Thorley, K. J.; Österholm, A. M.; Ponder, J. F., Jr.; Reynolds, J. R. Probing Comonomer Selection Effects on Dioxythiophene-Based Aqueous-Compatible Polymers for Redox Applications. *Chem. Mater.* **2022**, *34*, 4633−4645.
(50) Santiago-Adame, R.; Medina-Torres, L.; Gallegos-Infante, J. A.; Calderas, F.; González-Laredo, R. F.; Rocha-Guzmán, N. E.; Ochoa-Martínez, L. A.; Bernad-Bernad, M. J. Spray Drying-Microencapsulation of Cinnamon Infusions (Cinnamomum Zeylanicum) with Maltodextrin. *LWT - Food Science and Technology* **2015**, *64*, 571−577.
(51) Medina-Torres, L.; Nunez-Ramirez, D.; Calderas, F.; González-Laredo, R.; Minjares-Fuentes, J.; Valadez, M.; Bernad, M.; Manero, O. Microencapsulation of Gallic Acid by Spray Drying with Aloe Vera Mucilage (Aloe Barbadensis Miller) as Wall Material. *Ind. Crops Prod.* **2019**, *138*, No. 111461.
(52) Nafisifar, A.; Manshad, A. K.; Shadizadeh, S. R. Primary Evaluation of a New Green Synthesized Anionic Surfactant, Micellar Behavior Analysis, and Flooding in Sandstone Reservoirs: Application in Chemical Enhanced Oil Recovery. *SPE Journal* **2022**, *27*, 771−789.
(53) Nafisifar, A.; Khaksar Manshad, A.; Reza Shadizadeh, S. Evaluation of a New Green Synthesized Surfactant from Linseeds - Chemical EOR Implications from Sandstone Petroleum Reservoirs. *J. Mol. Liq.* **2021**, *342*, No. 117263.
(54) Hemmati, N.; Borazjani, S.; Yang, S.; Badalyan, A.; Genolet, L.; Behr, A.; Zeinijahromi, A.; Bedrikovetsky, P. Laboratory Validation of

Steady-State-Transient Test to Determine Relative Permeability and Capillary Pressure. *Fuel* **2022**, *321*, No. 123940.
(55) Al-Sarihi, A.; You, Z.; Behr, A.; Genolet, L.; Kowollik, P.; Zeinijahromi, A.; Bedrikovetsky, P. Admissible Parameters for Two-Phase Coreflood and Welge−JBN Method. *Transp Porous Media* **2020**, *131*, 831−871.
(56) Mirzaei-Paiaman, A.; Faramarzi-Palangar, M.; Djezzar, S.; Kord, S. A New Approach to Measure Wettability by Relative Permeability Measurements. *J Pet Sci Eng* **2022**, *208*, No. 109191.
(57) Berg, S.; Unsal, E.; Dijk, H. Non-Uniqueness and Uncertainty Quantification of Relative Permeability Measurements by Inverse Modelling. *Comput Geotech* **2021**, *132*, No. 103964.
(58) Chen, S.; Zhang, J.; Yin, D.; Cheng, X.; Jiang, N. Relative Permeability Measurement of Coal Microchannels Using Advanced Microchip Technology. *Fuel* **2022**, *312*, No. 122633.
(59) Higgs, S.; Da Wang, Y.; Sun, C.; Ennis-King, J.; Jackson, S. J.; Armstrong, R. T.; Mostaghimi, P. Direct Measurement of Hydrogen Relative Permeability Hysteresis for Underground Hydrogen Storage. *Int. J. Hydrogen Energy* **2023**, doi: DOI: 10.1016/j.ijhydene.2023.07.270.
(60) Minjares-Fuentes, J.; Femenia, A.; Comas-Serra, F.; Rodríguez-González, V. M. Compositional and Structural Features of the Main Bioactive Polysaccharides Present in the Aloe Vera Plant. *J. AOAC Int.* **2018**, *101*, 1711.
(61) Bajer, D.; Janczak, K.; Bajer, K. Novel Starch/Chitosan/Aloe Vera Composites as Promising Biopackaging Materials. *J Polym Environ* **2020**, *28*, 1021−1039.
(62) Meena, R. P.; Mandal, K.; Patel, M. P.; Minipara, D.; Samanta, J. N. Aetiology and Molecular Characterization of the Pathogens Associated with Soft Rot Disease of Aloe Vera (L.) Burm. f. *J Appl Res Med Aromat Plants* **2023**, *35*, No. 100492.
(63) Ikhou, D.; Guendouzi, A.; Kaid, M.; Ziani, H.; Villemin, D.; Chakraborty, A. Preparation and Characterization of Green Adsorbent on Functionalized and Nonfunctionalized ALOE VERA: A Combined Experimental and DFT Calculations. *Journal of the Indian Chemical Society* **2022**, *99*, No. 100544.
(64) Tang, H.; Han, Z.; Zhao, C.; Jiang, Q.; Tang, Y.; Li, Y.; Cheng, Z. Preparation and Characterization of Aloe Vera Polysaccharide-Based Packaging Film and Its Application in Blueberry Preservation. *Prog Org Coat* **2023**, *177*, No. 107445.
(65) Yılmaz, Ş.; Ecer, Ü.; Şahan, T. Synthesis, Characterization and Application of Iron-Supported Activated Carbon Derived from Aloe Vera Leaves to Improve Anaerobic Digestion of Food Waste: An Optimization Approach. *J Environ Chem Eng* **2023**, *11*, No. 110365.
(66) Taher, M. A.; Tan, W.-N.; Chear, N.J.-Y.; Leong, C.-R.; Rashid, S. A.; Tong, W.-Y. Metabolites Characterisation of Endophytic Phyllosticta Fallopiae L67 Isolated from Aloe Vera with Antimicrobial Activity on Diabetic Wound Microorganisms. *Nat Prod Res* **2023**, *37*, 1674−1679.
(67) Saha, J.; Mondal, Md.I.H.; Ahmed, F.; Rahman, M. Extraction, Characterization and Functionality Assessment of Aloe Vera, Chitosan and Silk Sericin. *Arabian Journal of Chemistry* **2023**, *16*, No. 105087.
(68) Hazarika, K.; Gogoi, S. B.; Kumar, A. Polymer Flooding and Its Effects on Enhanced Oil Recovery Special Reference to Upper Assam Basin. *Petroleum Research* **2023**, *8*, 54−62.
(69) Tackie-Otoo, B. N.; Ayoub Mohammed, M. A.; Otchere, D. A.; Jufar, S. R. A Study of the Oil Recovery Potential and Mechanisms of an Alternative Alkaline-Surfactant-Polymer Formulation for Carbonate Reservoir. *Geoenergy Science and Engineering* **2023**, *227*, No. 211881.
(70) Zhang, G.; Yu, J. Effect of Commonly Used EOR Polymers on Low Concentration Surfactant Phase Behaviors. *Fuel* **2021**, *286*, No. 119465.
(71) Nowrouzi, I.; Mohammadi, A. H.; Khaksar Manshad, A. A Natural Polymer Extracted from Chia Seeds for Application in Chemical Enhanced Oil Recovery by Taper Polymer Concentration (TPC) and Alkali-Polymer (AP) Slug Injection into Sandstone Oil Reservoirs. *Fuel* **2023**, *350*, No. 128738.
(72) Keykhosravi, A.; Vanani, M. B.; Aghayari, C. TiO2 Nanoparticle-Induced Xanthan Gum Polymer for EOR: Assessing the Underlying Mechanisms in Oil-Wet Carbonates. *J Pet Sci Eng* **2021**, *204*, No. 108756.
(73) Chauhan, G.; Verma, A.; Das, A.; Ojha, K. Rheological Studies and Optimization of Herschel-Bulkley Flow Parameters of Viscous Karaya Polymer Suspensions Using GA and PSO Algorithms. *Rheol. Acta* **2018**, *57*, 267.
(74) Shahrabadi, A.; Daghbandan, A.; Arabiyoun, M. Experimental Investigation of the Adsorption Process of the Surfactant-Nanoparticle Combination onto the Carbonate Reservoir Rock Surface in the Enhanced Oil Recovery (EOR) Process. *Chemical Thermodynamics and Thermal Analysis* **2022**, *6*, No. 100036.
(75) Tafur, N.; Somoza, A.; Muñuzuri, A. P.; Rodríguez-Cabo, B.; Barrio, I.; Panadero, A.; García-Mayoral, M. F.; Soto, A. Assessment of a Surface-Active Ionic Liquid Formulation for EOR Applications: Experimental and Simulation Studies. *Geoenergy Science and Engineering* **2023**, *224*, No. 211619.
(76) Tan, F.; Liu, W.; Ma, C.; Cheng, H.; Li, X.; Zhang, C. Classification Methods of Conglomerate Reservoirs Based on the Adsorption and Retention Law of Surfactant-Polymer Binary Systems. *J Pet Sci Eng* **2022**, *208*, No. 109195.
(77) Lee, Y.; Sung, W.; Wang, J. Polymer Efficiency and Sulfate Concentration for Hybrid EOR Application to an Acidic Carbonate Reservoir. *Pet Sci* **2023**, *20*, 993−1004.
(78) Zhao, L.; Guo, Y.; Azdarpour, A.; Mohammadian, E.; Norouzpour, M.; Liu, B. Synergism of a Novel Bio-Based Surfactant Derived from Pisum Sativum and Formation Brine for Chemical Enhanced Oil Recovery in Carbonate Oil Reservoirs. *Processes* **2023**, *11*, 1361.
(79) Mirzaei-Paiaman, A. New Methods for Qualitative and Quantitative Determination of Wettability from Relative Permeability Curves: Revisiting Craig's Rules of Thumb and Introducing Lak Wettability Index. *Fuel* **2021**, *288*, No. 119623.
(80) Naziri Mehrabani, S. A.; Vatanpour, V.; Koyuncu, I. Green Solvents in Polymeric Membrane Fabrication: A Review. *Sep Purif Technol* **2022**, *298*, No. 121691.
(81) Jadhawar, P.; Saeed, M. Low Salinity Water and Polymer Flooding in Sandstone Reservoirs: Upscaling from Nano-to Macro-Scale Using the Maximum Energy Barrier. *J Pet Sci Eng* **2023**, *220*, No. 111247.
(82) Ali, J. A.; Kolo, K.; Manshad, A. K.; Stephen, K. D. Potential Application of Low-Salinity Polymeric-Nanofluid in Carbonate Oil Reservoirs: IFT Reduction, Wettability Alteration, Rheology and Emulsification Characteristics. *J. Mol. Liq.* **2019**, *284*, 735−747.

https://doi.org/10.1021/acsomega.3c05921
ACS Omega 2023, 8, 43930−43954